

The Evolutionary Design of Collective Computation in Cellular Automata

James P. Crutchfield[†]
Santa Fe Institute
1399 Hyde Park Road
Santa Fe, NM 87501
chaos@santafe.edu

Melanie Mitchell
Santa Fe Institute
1399 Hyde Park Road
Santa Fe, NM 87501
mm@santafe.edu

Rajarshi Das[‡]
Center for Nonlinear Studies
Los Alamos Nat'l Laboratory
Los Alamos, NM 87545
raja@cnls.lanl.gov

[†]also Physics Department, University of California, Berkeley, CA 94720

[‡]also IBM Watson Research Center, P.O. Box 704, Yorktown Heights, NY 10598

Abstract. We investigate the ability of a genetic algorithm to design cellular automata that perform computations. The computational strategies of the resulting cellular automata can be understood using a framework in which “particles” embedded in space-time configurations carry information and interactions between particles effect information processing. This structural analysis can also be used to explain the evolutionary process by which the strategies were designed by the genetic algorithm. More generally, our goals are to understand how machine-learning processes can design complex decentralized systems with sophisticated collective computational abilities and to develop rigorous frameworks for understanding how the resulting dynamical systems perform computation.

Contents

1	Introduction	2
2	Cellular Automata	4
3	A Computational Task for Cellular Automata	6
4	Evolving Cellular Automata with Genetic Algorithms	9
5	Results of Experiments	10
5.1	Default Strategies	10
5.2	Block-Expanding Strategies	11
5.3	Embedded-Particle Strategies	11
6	Understanding Collective Computation in Cellular Automata	15
6.1	Computational Mechanics of Cellular Automata	17

6.2	Computational Mechanics of Evolved Cellular Automata	19
6.3	Computational Strategy of $\phi_{\text{par}}^{\text{a}}$	21
6.4	Computational Strategy of $\phi_{\text{par}}^{\text{b}}$ —Failure Analysis	26
7	Significance of the Particle-Level Description	27
8	Evolutionary History of $\phi_{\text{par}}^{\text{a}}$: Innovation, Contingency, and Exaptation	29
8.1	ϕ_{7b} and ϕ_8 (Fig. 14)	31
8.2	ϕ_8 and ϕ_{13} (Fig. 15)	32
8.3	ϕ_{13} and ϕ_{17} (Fig. 16)	33
8.4	ϕ_{17} and ϕ_{18} (Fig. 17)	34
8.5	ϕ_{18} and ϕ_{33} (Fig. 18)	35
8.6	ϕ_{33} and ϕ_{64} (Fig. 19)	35
8.7	Particle Models of Evolved Cellular Automata	36
9	Related Work	37
10	Conclusion	40
A	Domain Filter	42

1. Introduction

From the earliest days of computer science, researchers have been interested in making computers and computation more like information-processing systems in nature. In the 1940’s and 1950’s, von Neumann viewed the new field of “automata theory” as closely related to theoretical biology, and asked questions such as “How are computers and brains alike?” [75] and “What is necessary for an automaton to reproduce itself?” [76]. Turing was deeply interested in the mechanical roots of human-like intelligence [72], and Weiner looked for links among the functioning of computers, nervous systems, and societies [79]. More recently work on biologically and sociologically inspired computation has received renewed interest; researchers are borrowing information-processing mechanisms found in natural systems such as brains [7, 28, 63], immune systems [26, 31], insect colonies [9, 21], economies [78, 80], and biological evolution [2, 29, 40]. The motivation behind such work is both to understand how systems in nature adaptively process information and to construct fast, robust, adaptive computational systems that can learn on their own and perform well in many environments.

Although there are some commonalities, natural systems differ considerably from traditional von Neumann-style architectures¹. Biological systems such as brains, immune systems,

¹It should be noted that although computer architectures with central control, random access memory,

and insect societies consist of myriad relatively homogeneous components that are extended in space and operate in parallel with no central control and with only limited communication among components. Information processing in such systems arises from coordination among large-scale patterns that are distributed across components (e.g., distributed activations of neurons or activities of antibodies). Such decentralized systems, being highly nonlinear, often exhibit complicated, difficult-to-analyze, and unpredictable behavior. The result is that they are hard to control and “program”. It seems clear that in order to design and understand decentralized systems and to develop them into useful technologies, engineers must extend traditional notions of computation to encompass these architectures. This has been done to some extent in research on parallel and distributed computing (e.g., [10]) and with architectures such as systolic arrays [47]. However, as computing systems become more parallelized and decentralized and employ increasingly simple individual processors, it becomes harder and harder to design and program such systems.

Cellular automata (CAs) are a simple class of systems that captures some of the features of systems in nature listed above: large numbers of homogeneous components (simple finite state machines) extended in space, no central control, and limited communication among components. Given that there is no programming paradigm for implementing parallel computations in CAs, our research investigates how genetic algorithms (GAs) can evolve CAs to perform computations requiring coordination among many cells. In other words, the GA’s job is to design ways in which the actions of simple components with local information and communication give rise to coordinated global information processing. In addition, we have adapted a framework—“computational mechanics”—that can be used to discover how information processing is embedded in dynamical systems [12] and thus to analyze how computation emerges in evolved CAs. Our ultimate motivations are two-fold: (i) to understand collective computation and its evolution in natural systems and (ii) to explore ways of automatically engineering sophisticated collective computation in decentralized multi-processor systems.

In previous work we described some of the mechanisms by which genetic algorithms evolve cellular automata to perform computations, and some of the impediments faced by the GA [56]. We also briefly sketched our adaptation of the computational mechanics approach to understanding computation in the evolved CAs [17, 19, 20]. In this paper we give a more fully developed account of our research to date on these topics, report on new results, and compare our work with other work on GAs, CAs, and distributed computing.

This paper is organized as follows. In Sec. 2–4, we review cellular automata, define a computational task for CAs—“density classification”—that requires global coordination, and describe how we used a GA to evolve cellular automata to perform this task. In Sec. 5–8, we describe the results of the GA evolution of CAs. We first describe the different types of CA computational strategies discovered by the GA for performing the density classification task. We then make the notion of computational “strategies” more rigorous by defining them in terms of embedded particles, particle interactions, and geometric “subroutines” consisting of these components. This high-level description enables us to explain how the space-time configurations generated by the evolved CAs give rise to collective computation and to predict quantitatively the CAs’s computational performance. We then use embedded-

and serial processing have been termed “von Neumann style”, von Neumann was also one of the inventors of “non von Neumann-style” architectures such as cellular automata.

Rule table ϕ :

Neighborhood η : 000 001 010 011 100 101 110 111
 Output bit $\phi(\eta)$: 0 1 1 1 0 1 1 0

Lattice configuration:

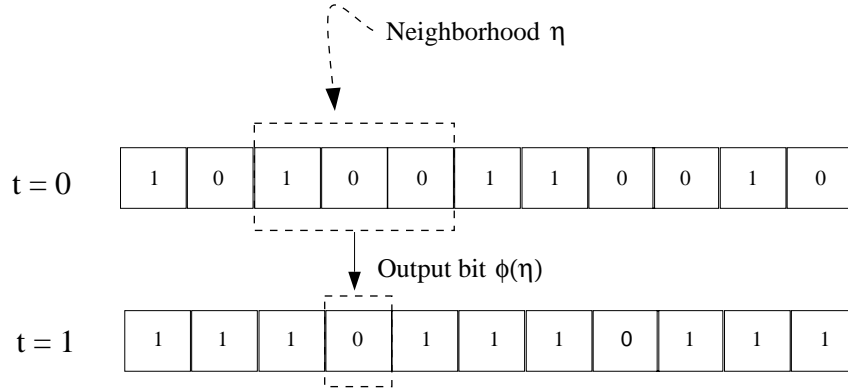


Figure 1: The components of one-dimensional, binary-state, $r = 1$ (“elementary”) CA 110 shown iterated one time step on a configuration with $N = 11$ lattice sites and periodic boundary conditions (i.e., $s_N = s_0$).

particle descriptions to explain the evolutionary stages by which the successful CAs were produced by the GA. Finally, in Sec. 9 we compare our research with related work.

2. Cellular Automata

An one-dimensional cellular automaton consists of a lattice of N identical finite-state machines (*cells*), each with an identical topology of local connections to other cells for input and output, along with boundary conditions. Let Σ denote the set of states in a cell’s finite-state machine and let $k = |\Sigma|$ denote the number of states per cell. Each cell is indexed by its site number $i = 0, 1, \dots, N - 1$. A cell’s state at time t is denoted by s_i^t , where $s_i^t \in \Sigma$. The state s_i^t of cell i together with the states of the cells to which it is connected is called the *neighborhood* η_i^t of cell i . Each cell obeys the same transition rule $\phi(\eta_i^t)$, that gives the update state $s_i^{t+1} = \phi(\eta_i^t)$ for cell i as a function of η_i^t . We will drop the indices on s_i^t and η_i^t when we refer to them as general (local) variables.

We use \mathbf{s}^t to denote the *configuration* of cell states:

$$\mathbf{s}^t = s_0^t s_1^t \dots s_{N-1}^t.$$

A CA $\{\Sigma^N, \phi\}$ thus specifies a global map Φ of the configurations:

$$\Phi : \Sigma^N \rightarrow \Sigma^N,$$

with

$$\mathbf{s}^{t+1} = \Phi(\mathbf{s}^t).$$

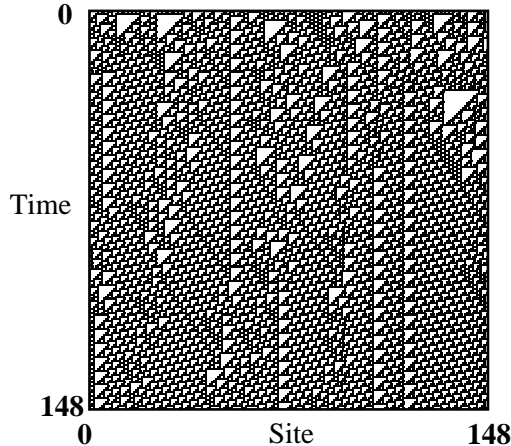


Figure 2: A space-time diagram illustrating the typical behavior of elementary CA (ECA) 110. The lattice of 149 sites, displayed horizontally at the top, starts with \mathbf{s}_0 being an arbitrary initial configuration. Cells in state 1 are displayed as black and cells in state 0 are displayed as white. Time increases down the page.

In some cases in the discussion below, Φ will also be used to denote a map on subconfigurations of the lattice. Whether Φ applies to global configurations or subconfigurations should be clear from context.

In a *synchronous CA*, a global clock provides an update signal for all cells: at each t all cells synchronously read the states of the cells in their neighborhood and then update their own states according to $s_i^t = \phi(\eta_i^t)$.

The neighborhood η is often taken to be spatially symmetric. For one-dimensional CAs, $\eta_i = s_{i-r}, \dots, s_0, \dots, s_{i+r}$, where r is the CA's *radius*. Thus, $\phi : \Sigma^{2r+1} \rightarrow \Sigma$. For small-radius, binary-state CAs, in which the number of possible neighborhoods is not too large, ϕ is often displayed as a look-up table, or *rule table*, that lists each possible η together with its resulting *output bit* s^{t+1} .

The architecture of a one-dimensional, $(k, r) = (2, 1)$ CA is illustrated in Fig. 1. Here, the neighborhood of each cell consists of itself and its two nearest neighbors and the boundary conditions are periodic: $s_N = s_0$.

The 256 one-dimensional, $(k, r) = (2, 1)$ CAs are called *elementary CAs* (ECAs). Wolfram [81] introduced a numbering scheme for one-dimensional CAs. The output bits can be ordered lexicographically, as in Fig. 1, and are interpreted as the binary representation of an integer between 0 and 255 with the leftmost bit being the least-significant digit and the rightmost the most-significant digit. In this scheme, the elementary CA pictured here is number 110.

In this paper we will restrict our attention to synchronous, one-dimensional, $(k, r) = (2, 3)$ CAs with periodic boundary conditions. This choice of parameters will be explained below. For ease of presentation, we will sometimes refer to a CA by its transition rule ϕ (e.g., as in “the CA ϕ ...”).

The behavior of CAs is often illustrated using space-time diagrams in which the con-

figurations \mathbf{s}^t on the lattice are plotted as a function of time. Fig. 2 shows a space-time diagram of the behavior of ECA 110 on a lattice of $N = 149$ sites and periodic boundary conditions, starting from an arbitrary initial configuration (the lattice is displayed horizontally) and iterated over 149 time steps with time increasing down the figure. A variety of local structures are apparent to the eye in the space-time diagram. They develop over time and move in space and interact.

ECAs are among the simplest spatial dynamical systems: discrete in time, space, and local state. Despite this, as can be seen in Fig. 2, they generate quite complicated, even apparently aperiodic behavior. The architecture of a CA can be modified in many ways—increasing the number of spatial dimensions, the number k of states per cell, and the neighborhood size r ; modifying the boundary conditions; making the local CA rule ϕ probabilistic rather than deterministic; making the global update Φ asynchronous; and so on.

CAs are included in the general class of “iterative networks” or “automata networks”. (See [30] for a review.) They are distinguished from other architectures in this class by their homogeneous and local ($r \ll N$) connectivity among cells, homogeneous update rule across all cells, and (typically) relatively small k .

For quite some time, due to their appealingly simple architecture, CAs have been successfully employed as models of physical, chemical, biological, and social phenomena, such as fluid flow, galaxy formation, earthquakes, chemical pattern formation, biological morphogenesis, and vehicular traffic dynamics. They have been considered as mathematical objects about which formal properties can be proved. They have been used as parallel computing devices, both for the high-speed simulation of scientific models and for computational tasks such as image processing. In addition, CAs have been used as abstract models for studying “emergent” cooperative or collective behavior in complex systems. For discussions of work in all these areas, see, e.g., [4, 25, 30, 37, 46, 59, 44, 55, 71, 82].

3. A Computational Task for Cellular Automata

It has been shown that some CAs are capable of universal computation; see, e.g., [3, 50, 67]. The constructions either embed a universal Turing machine’s tape states, read/write head location, and finite-state control in a CA’s configurations and rule or they design a CA rule, supporting propagating and interacting particles, that simulates a universal logic circuit. These constructions are intended to be in-principle demonstrations of the potential computational capability of CAs, rather than implementations of practical computing devices; they do not give much insight about the computational capabilities of CAs in practice. Also, in such constructions it is typically very difficult to design initial configurations that perform a desired computation. Moreover, these constructions amount to using a massively parallel architecture to simulate a serial one.

Our interest in CA computation is quite different from this approach. In our work, CAs are considered to be massively parallel and spatially extended pattern-forming systems. Our goal is to use machine-learning procedures, such as GA stochastic search, to automatically design CAs that implement parallel computation by taking advantage of the patterns formed via collective behavior of the cells.

To this end, we chose a particular computation for a one-dimensional, binary-state CA—density classification—that requires collective behavior. The task is to determine whether ρ_0 , the fraction of 1s in the initial configuration (IC) \mathbf{s}_0 , is greater than or less than a critical value ρ_c . If $\rho_0 > \rho_c$, the entire lattice should relax to a fixed point of all 1s (i.e., $\Phi(1^N) = 1^N$) in a maximum of T_{\max} time steps; otherwise it should relax to a fixed point of all 0s (i.e., $\Phi(0^N) = 0^N$) within that time. The task is undefined for $\rho_0 = \rho_c$. In our experiments we set $\rho_c = 1/2$ and $T_{\max} = 2N$. The *performance* $\mathcal{P}_N^I(\phi)$ of a CA ϕ on this task is calculated by randomly choosing I initial configurations on a lattice of N cells, iterating ϕ on each IC for a maximum of T_{\max} time steps, and determining the fraction of the I ICs that were correctly classified by ϕ —a fixed point of all 1s for $\rho_0 > \rho_c$, and a fixed point of all 0s otherwise. No partial credit is given for final configurations that have not reached an all-1s or all-0s fixed point. As a shorthand, we will refer to this task as the “ $\rho_c = 1/2$ ” task. Defining the task for other values of ρ_c is of course possible; e.g., Chau et al. showed that it is possible to perform the task for rational densities ρ_c using two one-dimensional elementary CAs in succession [6].

This task is trivial for a von Neumann-style architecture that holds the IC as an array in memory: it simply requires counting the number of 1s in \mathbf{s}_0 . It is also trivial for a two-layer neural network presented with each s_i^0 on one of its N input units, all of which feed into a single output unit: it simply requires weights set so that the output unit fires when the activation reaches the desired threshold ρ_c . In contrast, it is nontrivial to design a CA of our type to perform this task: all cells must agree on a global characteristic of the input even though each cell communicates its state only to its neighbors.

The $\rho_c = 1/2$ task for CAs can be contrasted with the well-studied tasks known as “Byzantine agreement” and “consensus” in the distributed computing literature (e.g., [22, 27]). These are tasks requiring a number of distributed processors to come to agreement on a particular value held initially by one of the processors. Many decentralized protocols have been developed for such tasks. They invariably assume that the individual processors have more sophisticated computational capabilities and memory than the individual cells in our binary-state CAs or that the communication topologies are more complicated than that of our CAs. Moreover, to our knowledge, none of these protocols addresses the problem of classifying a global property (such as initial density) of all the processors.

Given this background, we asked whether a GA could design CAs in which collective behavior allowed them to perform well above chance ($> \mathcal{P}_N^I(\phi) = 0.5$) on this task for a range of N . To minimize local processor and local communication complexity, we wanted to use the smallest values of k and r for which such behavior could be obtained. Over all 256 ECAs ϕ , the maximum performance $\mathcal{P}_N^{10^4}(\phi)$ is approximately 0.5 for $N \in \{149, 599, 999\}$. For all CAs ϕ evolved in 300 runs of the GA on $(k, r) = (2, 2)$ CAs, the maximum $\mathcal{P}_N^{10^4}(\phi)$ was approximately 0.58 for $N = 149$ and approximately 0.5 for $N \in \{599, 999\}$. (The GA’s details will be given in the next section.) Increasing the radius to $r = 3$, though, resulted in markedly higher performance and more sophisticated collective behavior. As a result, all of the experiments described in this paper were performed on one-dimensional $(k, r) = (2, 3)$ CAs with $N \in \{149, 599, 999\}$ and periodic boundary conditions. Note that for $r = 3$, the neighborhood size $|\eta| = 7$.

One naive candidate solution to the $\rho_c = 1/2$ task, which we will contrast with the

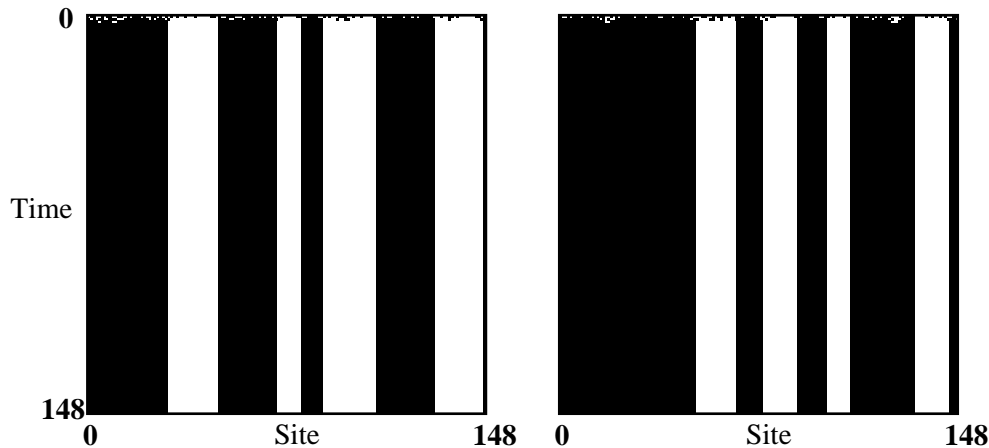


Figure 3: Space-time diagrams for ϕ_{maj} , the $r = 3$ local-majority-vote CA. In the left diagram, $\rho_0 < 1/2$; in the right diagram, $\rho_0 > 1/2$.

GA-evolved CAs, is the $r = 3$ “majority vote” CA. This CA, denoted ϕ_{maj} , maps the center cell in each 7-cell neighborhood to the majority state in that neighborhood. Fig. 3 gives two space-time diagrams illustrating the behavior of ϕ_{maj} on two ICs, one with $\rho_0 < 1/2$ and the other with $\rho_0 > 1/2$. As can be seen, small high-density (low-density) regions are mapped to regions of all 1s (0s). But when an all-1s region and an all-0s region border each other, there is no way to decide between them and both persist. Thus, ϕ_{maj} does not perform the $\rho_c = 1/2$ task. In particular, $\mathcal{P}_N^{10^4}(\phi_{\text{maj}})$ was measured to be zero for $N \in \{149, 599, 999\}$. At a minimum more sophisticated coordination in the form of information transfer and decision making is required. And, given the local nature of control and communication in CAs, the coordination among cells must emerge in the absence of any central processor or central memory directing the cells.

Other researchers, building on our work, have examined variations of the $\rho_c = 1/2$ task that can be performed by simple CAs or by combinations of CAs. Capcarrere et al. [5] noted that changing the output specification makes the task significantly easier. For example, ECA 184 classifies densities of initial conditions within $\lceil N/2 \rceil$ time steps by producing a final configuration of a checkerboard pattern $(01)^*$ interrupted by one or more blocks of at least two consecutive 0s for low-density ICs or at least two consecutive 1s for high-density ICs. Fuks [32] noted that by using the final configuration of ECA 184 as the initial configuration of ECA 232, the correct final configuration of either all-0s or all-1s is obtained. Note that Fuks’ solution requires a central controller that counts time up to $\lceil N/2 \rceil$ steps in order to shift from a CA using rule 184 to one using rule 232.

Both solutions always yield correct density classification, whereas the single-CA $\rho_c = 1/2$ task is considerably more difficult. In fact, it has been proven that no single, finite-radius two-state CA can perform the $\rho_c = 1/2$ task perfectly for all N [18, 48].

Our interest is not focused on developing a new and better parallel method for performing this specific task. Clearly, one-dimensional, binary-state cellular automata are far from the best architectures to use if one is interested in performing density classification efficiently. As we have emphasized before, the task is trivial within other computational model classes. Instead, our interest is in investigating how GAs can design CAs that have

interesting collective computational capabilities and how we can understand those capabilities. Due to our more general interest, we have been able to adapt this paradigm to other spatial computation tasks—tasks for which the above specific solutions do not apply and for which even approximate hand-designed CA solutions were not previously known [19].

4. Evolving Cellular Automata with Genetic Algorithms

Genetic algorithms are search methods inspired by biological evolution [40]. In a typical GA, candidate solutions to a given problem are encoded as bit strings. A population of such strings (“chromosomes”) is chosen at random and evolves over several generations under selection, crossover, and mutation. At each generation, the fitness of each chromosome is calculated according to some externally imposed fitness function and the highest-fitness chromosomes are selected preferentially to form a new population via reproduction. Pairs of such chromosomes produce offspring via crossover, where an offspring receives components of its chromosome from each parent. The offspring chromosomes are then subject at each bit position to a small probability of mutation (i.e., being flipped). After several generations, the population often contains high-fitness chromosomes—approximate solutions to the given problem. (For overviews of GAs, see [35, 54].)

We used a GA to search for $(k, r) = (2, 3)$ CAs to perform the $\rho_c = 1/2$ task.² Each chromosome in the population represented a candidate CA—it consisted of the output bits of the rule table, listed in lexicographic order of neighborhood (cf. ϕ in Fig. 1). The chromosomes representing CAs were of length $2^{2r+1} = 128$ bits. The size of the space in which the GA searched was thus 2^{128} —far too large for exhaustive enumeration and performance evaluation.

Our version of the GA worked as follows.

First, an initial population of M chromosomes was chosen at random. The *fitness* $F_N^I(\phi)$ of a CA ϕ in the population was computed by randomly choosing I ICs on a lattice of N cells, iterating the CA on each IC either until it arrived at a fixed point or for a maximum of T_{\max} time steps. It was then determined whether the final configuration was correct—i.e., the all-0s fixed point for $\rho_0 < 1/2$ or the all-1s fixed point for $\rho_0 > 1/2$. $F_N^I(\phi)$ was the fraction of the I ICs on which ϕ produced the correct final behavior. No credit was given for partially correct final configurations.

In each generation, (1) a new set of I ICs was generated; (2) $F_N^I(\phi)$ was computed for each CA ϕ in the population; (3) CAs in the population were ranked in order of fitness (with ties broken at random); (4) a number E of the highest fitness CAs (the “elite”) was copied to the next generation without modification; and (5) the remaining $M - E$ CAs for the next generation were formed by crossovers between randomly chosen pairs of the elite CAs. With probability p_c , each pair was crossed over at a single randomly chosen locus l , forming two offspring. The first child inherited bits 0 through l from the first parent and bits $l + 1$ through 127 from the second parent; vice versa for the second child. The parent CAs were chosen for crossover from the elite with replacement—that is, an elite CA was permitted to be chosen any number of times. The two offspring chromosomes from each crossover (or copies of the

²The basic framework was introduced in Ref. [61] to study issues of phase transitions, computation, and adaptation. For a review of the original motivations and a critique of the results see Ref. [57].

parents, if crossover did not take place) were mutated ($0 \rightarrow 1$ and $1 \rightarrow 0$) at each locus with probability p_m . This process was repeated for G generations during a single GA run. Note that since a different sample of ICs was chosen at each generation, the fitness function itself is a random variable.

We ran experiments with two different distributions for choosing the M chromosomes in the initial population and the set of I ICs at each generation: (i) an “unbiased” distribution in which each bit’s value is chosen independently with equal probability for 0 and 1, and (ii) a density-uniform distribution in which strings were chosen with uniform probability over $\lambda \in [0, 1]$ or over $\rho_0 \in [0, 1]$, where λ is the fraction of 1s in ϕ ’s output bits and ρ_0 is the fraction of 1s in the IC. Using the density-uniform distribution for the initial CA population and for the ICs considerably improved the GA’s ability to find high fitness CAs on any given run. (That is, we could use 50% fewer generations per GA run and still find high performance CAs.) The results we report here are from experiments in which density-uniform distributions were used.

The experimental parameters we used were $M = 100$, $I = 100$, $E = 20$, $N = 149$, $T_{\max} = 2N$, $p_c = 1.0$ (i.e., crossover was always performed), $p_m = 0.016$, and $G = 100$. Experiments using variations on these parameters did not result in higher performance solutions or faster convergence to the best-performance solutions.

To test the quality of the evolved CAs we used $\mathcal{P}_N^{10^4}$ with $N \in \{149, 599, 999\}$. This performance measure is a more stringent quality test than the fitness F_N^{100} used in the GA runs: under $\mathcal{P}_N^{10^4}$ the ICs are chosen from an unbiased distribution and thus have ρ_0 close to the density threshold $\rho = 1/2$. Such ICs are the hardest cases to classify. Thus, $\mathcal{P}_N^{10^4}$ gives a lower bound on other performance measures. In machine learning terms, the ICs used to calculate F_{149}^{100} are the training sets for the CAs and the ICs used to calculate $\mathcal{P}_N^{10^4}$ are larger and harder test sets that probe the evolved CA’s generalization ability.

5. Results of Experiments

In this section we describe the results from 300 independent runs of this GA, with different random number seeds.

In each of the 300 runs, the population converged to CAs implementing one of three types of computational strategies. The term “strategy” here refers to the mechanisms by which the CA attains some level of fitness on the $\rho_c = 1/2$ task. These three strategy types, “default”, “block expanding”, and “particle”, are illustrated in Figures 4–6. In each figure, each row contains two space-time diagrams displaying the typical behavior of a CA ϕ that was evolved in a GA run. Thus, CAs from six different runs are shown. In each row, $\rho_0 < 1/2$ in the left space-time diagram and $\rho_0 > 1/2$ in the right. The rule tables and measured $\mathcal{P}_N^{10^4}$ values for the six CAs are given in Table 1.

5.1 Default Strategies

In 11 out of the 300 runs, the highest performance CAs implemented “default” strategies, which on almost all ICs iterate to all 0s or all 1s, respectively. The typical behavior of two

such CAs, $\phi_{\text{def}}^{\text{a}}$ and $\phi_{\text{def}}^{\text{b}}$, is illustrated in Figures 4(a) and 4(b). Default strategies each have $\mathcal{P}_N^I(\phi) \approx 0.5$, since each classifies one density range (e.g., $\rho < 1/2$) correctly and the other ($\rho > 1/2$) incorrectly. Since the initial CA population is generated with uniform distribution over λ it always contains some CAs with very high or low λ . And since λ is the fraction of 1s in the output bits of the look-up table, these extreme- λ CAs tend to have one or the other default behavior.

5.2 Block-Expanding Strategies

In most runs (280 out of 300 in our experiments) the GA evolved CAs with strategies like those shown in Figures 5(a) and 5(b). $\phi_{\text{exp}}^{\text{a}}$ in Fig. 5(a) defaults to an all-1s fixed point (right diagram) unless there is a sufficiently large block of adjacent (or almost adjacent) 0s in the IC. In this case it expands that block until 0s fill up the entire lattice (left diagram). $\phi_{\text{exp}}^{\text{b}}$ in Fig. 5(b) has the opposite strategy. It defaults to the all-0s fixed point unless there is a sufficiently large block of 1s in the IC. The meaning of “sufficiently large block” depends on the particular CA, but is typically close to the neighborhood size $2r + 1$. For example, $\phi_{\text{exp}}^{\text{a}}$ will expand blocks of 8 or more 0s and $\phi_{\text{exp}}^{\text{b}}$ will expand blocks of 7 or more 1s.

These “block-expanding” strategies rely on the presence or absence of blocks of 1s or 0s in the IC: blocks of adjacent 0s (1s) are more likely to appear in low- (high-) density ICs. Since the occurrence of such blocks is statistically correlated with ρ_0 , recognizing and then expanding them leads to fitnesses above those for the default strategy. The strength of this correlation depends on the initial density ρ_0 and on the lattice size N . Typical block-expanding strategies have $F_{149}^{100} \approx 0.9$ and $\mathcal{P}_{149}^{10^4} \approx 0.6$. The block-expanding strategies designed by the GA are adapted to $N = 149$; their performances do not scale well to larger lattice sizes. This occurs since the probability of a block of, say, seven adjacent 1s appearing for a given ρ_0 increases with N and this means that the correlation between the occurrence of this block and density decreases. This can be seen in the measured values of $\mathcal{P}_N^{10^4}$ for $\phi_{\text{exp}}^{\text{a}}$ and $\phi_{\text{exp}}^{\text{b}}$ for longer lattices given in Table 1.

5.3 Embedded-Particle Strategies

The block-expanding strategies are not examples of the kind of sophisticated coordination and information transfer that we claimed must be achieved for robust performance on the $\rho_c = 1/2$ task. Under these strategies all the computation is done locally in identifying and then expanding a “sufficiently large” block. Moreover, the performance on $N = 149$ does not generalize to larger lattices. Clearly, the block-expanding strategies are missing important aspects required by the task. The third class of strategies evolved by the GA, the “embedded-particle” strategies, do achieve the coordination and communication we alluded to earlier. Typical space-time behaviors of two particle strategies, $\phi_{\text{par}}^{\text{a}}$ and $\phi_{\text{par}}^{\text{b}}$, are given in Figures 6(a) and 6(b). It can be seen that there is a transient phase during which the spatial and temporal transfer of information about the local density takes place. Such strategies were evolved in 9 out of the 300 runs.

$\phi_{\text{par}}^{\text{a}}$ ’s behavior is somewhat similar to that of ϕ_{maj} in that local high-density regions are mapped to all 1s and local low-density regions are mapped to all 0s. In addition, a

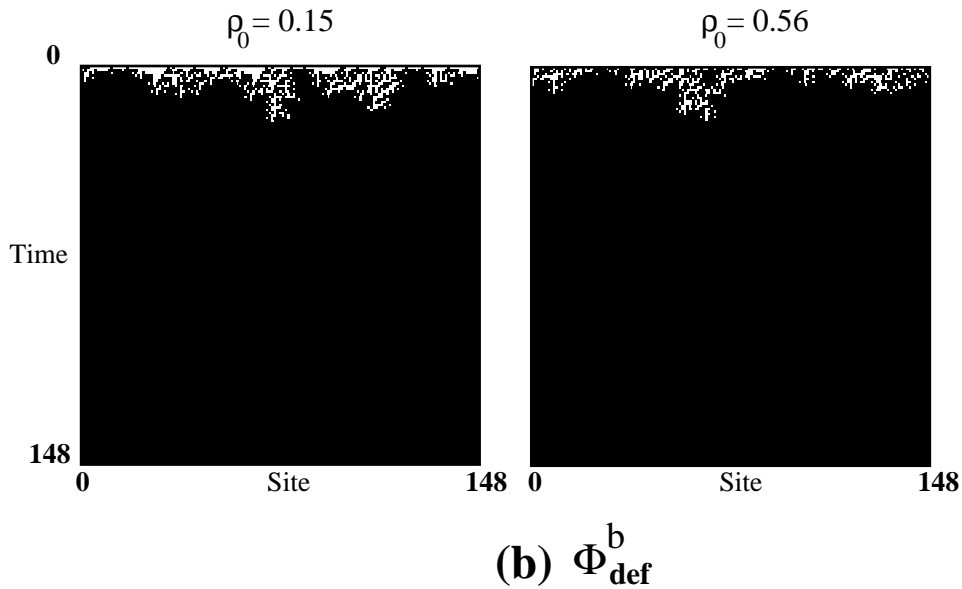
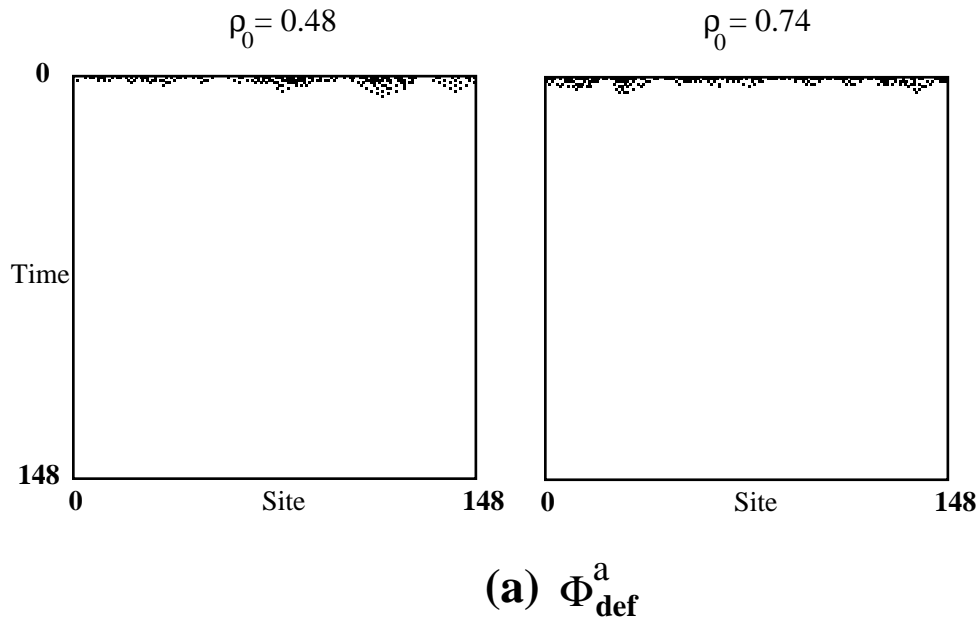


Figure 4: Space-time behavior of “default” strategy CAs evolved on two different GA runs. (a) ϕ_{def}^a with $\rho_0 = 0.48$ (left) and $\rho_0 = 0.74$ (right). On almost all ICs this CA iterates to a fixed point of all 0s, correctly classifying only low- ρ ICs. (b) ϕ_{def}^b with $\rho_0 = 0.15$ (left) and $\rho_0 = 0.56$ (right). On almost all ICs this CA iterates to a fixed point of all 1s, correctly classifying only high- ρ ICs.

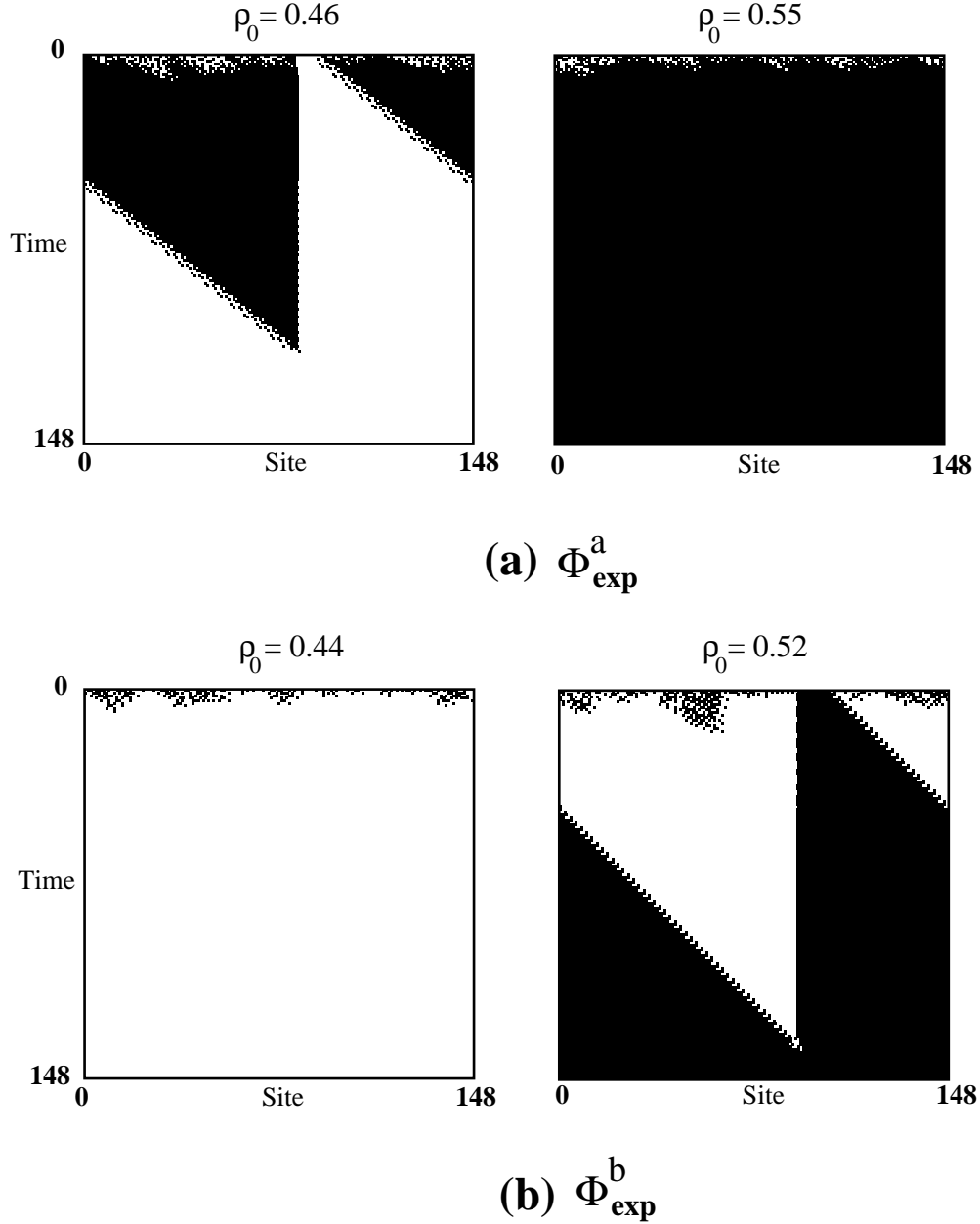


Figure 5: Space-time behavior of two “block expanding” CAs evolved on different GA runs. (a) ϕ_{exp}^a with $\rho_0 = 0.46$ (left) and $\rho_0 = 0.55$ (right). This CA defaults to a fixed point of all 1s unless the IC contains a sufficiently large block of adjacent 0s, in which case, that block is expanded. (b) ϕ_{exp}^b with $\rho_0 = 0.44$ (left) and $\rho_0 = 0.52$ (right). This CA defaults to a fixed point of all 0s unless the IC contains a sufficiently large block of adjacent 1s, in which case, that block is expanded. The classification of the IC is correct in each of these four cases.

vertical stationary boundary separates these regions. The set of local spatial configurations that make up this boundary is specified in formal language terms by the regular expression $(1)^+01(0)^+$, where $(w)^+$ means a positive number of repetitions of the word w [41].

The stationary boundary appears when a region of 1s on the left meets a region of 0s on the right. However, there is a crucial difference from ϕ_{maj} : when a region of 0s on the left meets a region of 1s on the right, a checkerboard region $(01)^+$ grows in size with equal speed in both directions. A closer analysis of its role in the overall space-time behavior shows that the checkerboard region serves to decide which of the two adjacent regions (0s and 1s) is the larger. It does this by simply cutting off the smaller region and so the larger (0 or 1) region continues to expand. The net decision is that the density in the region was in fact below or above $\rho_c = 1/2$. The spatial computation here is largely geometric: there is a competition between the sizes of high- and low-density regions.

For example, consider the right-hand space-time diagram of Fig. 6(a). The large low-density region between the lines marked “boundary 1” and “boundary 2” is smaller than the large high-density region between “boundary 2” and “boundary 1” (moving left from boundary 2 and wrapping around). The left-hand side of the checkerboard region (centered around boundary 2) collides with boundary 1 before the right-hand side does. The result is that the collision cuts off the inner white region, letting the outer black region propagate.

In this way, $\phi_{\text{par}}^{\text{a}}$ uses local interactions and simple geometry to determine the relative sizes of adjacent low- and high-density regions that are larger than the neighborhood size. As is evident in Figures 6(a) and 6(b), this type of size competition over time happens across increasingly larger spatial scales, gradually resolving competitions between larger and larger regions.

The black-white boundary and the checkerboard region can be thought of as signals indicating “ambiguous” density regions. Each of these boundaries has local density exactly at $\rho_c = 1/2$. Thus, they are not themselves “classified” by the CA as low or high density. The result is that these signals can persist over time. The creation and interaction of these signals can be interpreted as the locus of the computation being performed by the CA—they form its emergent “algorithm”, what we have been referring to as the CA’s “strategy”.

$\phi_{\text{par}}^{\text{b}}$ (Fig. 6(b)) follows a similar strategy, but with a vertically striped region playing the role of the checkerboard region in $\phi_{\text{par}}^{\text{a}}$. However, in this case there are asymmetries in the speeds of the propagating region boundaries. This difference yields a lower $\mathcal{P}_N^{10^4}$, as can be seen in Table 1.

These descriptions of the computational strategies evolved by the GA are informal. A major goal of our work is to make terms such as “computation”, “computational strategy”, and “emergent algorithm” more rigorous for cellular automata. In the next section we will describe how we are using the notions of domains, particles, and particle interactions to do this. We will use these notions to answer questions such as, How, precisely, is a given CA performing the task? What structural components are used to support this information processing? How can we predict \mathcal{P}_N^I and other computational properties of a given CA? Why is \mathcal{P}_N^I greater for one CA than for another? What types of mistakes does a given CA make in performing the $\rho_c = 1/2$ task? These types of questions are difficult, if not impossible, to answer in terms of local space-time notions such as the bits in a CA’s look-up table or even

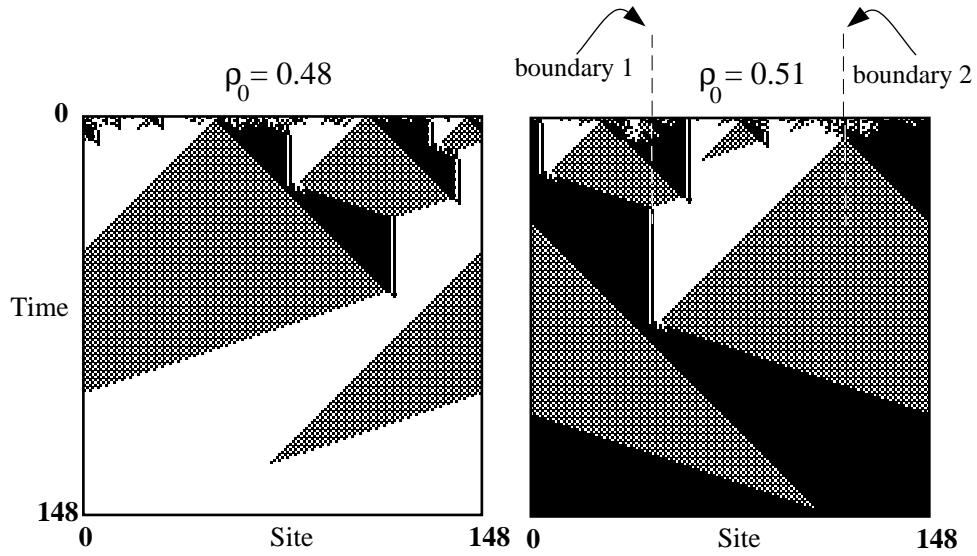
CA Name	Rule Table (Hexadecimal)	$\mathcal{P}_{149}^{10^4}$	$\mathcal{P}_{599}^{10^4}$	$\mathcal{P}_{999}^{10^4}$
$\phi_{\text{def}}^{\text{a}}$	100111215030114D 01613507143B05BF	0.500	0.500	0.500
$\phi_{\text{def}}^{\text{b}}$	0BF9D97AF26F4F4B F3FF301F0B110DF7	0.499	0.499	0.501
$\phi_{\text{exp}}^{\text{a}}$	1010614604273F9B 7FD7D9DF35F53FFF	0.656	0.523	0.504
$\phi_{\text{exp}}^{\text{b}}$	02330A4B07016711 42D080C3CD877B7F	0.643	0.513	0.502
$\phi_{\text{par}}^{\text{a}}$	0504058605000F77 037755877BFFB77F	0.775	0.740	0.728
$\phi_{\text{par}}^{\text{b}}$	00240066A0A02246 76EFEFFFFBFFAAFE	0.766	0.687	0.641

Table 1: CA chromosomes (look-up table output bits) given in hexadecimal and $\mathcal{P}_N^{10^4}$ for the six CAs illustrated in Figures 4–6, on lattices of sizes $N = 149$, $N = 599$, and $N = 999$. To recover the 128-bit string giving the CA look-up table outputs, expand each hexadecimal digit (left to right, top row followed by bottom row) to binary. This yields the neighborhood outputs in lexicographic order of neighborhood, with the leftmost bit of the 128-bit string giving the output bit for neighborhood 00000000, and so on. Since $\mathcal{P}_N^{10^4}$ is measured on a randomly chosen sample of ICs, it is a random variable. This table gives its mean over 100 trials for each CA. Its standard deviation over the same 100 trials is approximately 0.005 for each CA for all three values of N . For comparison, the best known $(k, r) = (2, 3)$ CAs for the $\rho_c = 1/2$ task have $\mathcal{P}_{149}^{10^4} \approx 0.85$ (see Sec. 9). This appears to be close to the upper limit of $\mathcal{P}_{149}^{10^4}$ for this class of spatial architectures.

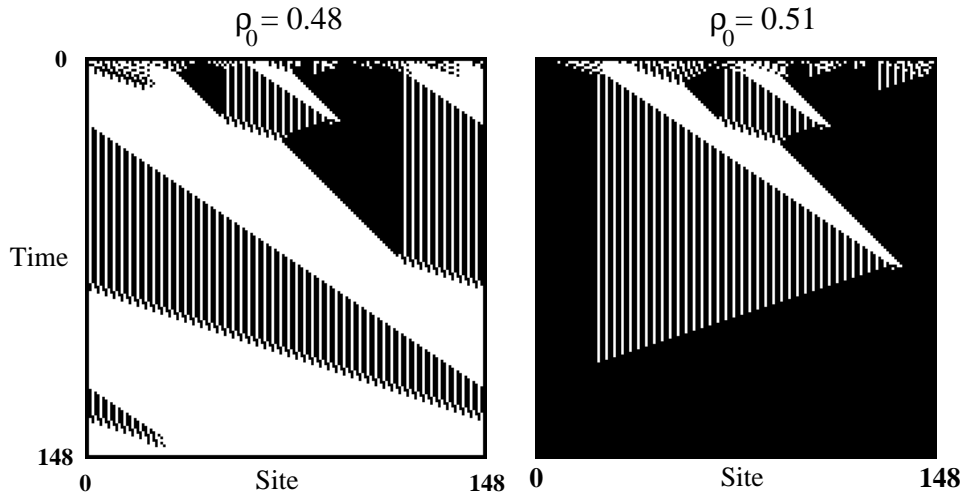
the raw space-time configurations produced by the CA. A higher-level description is needed, one that incorporates computational structures.

6. Understanding Collective Computation in Cellular Automata

In this section we will describe our approach to formalizing the notion of computational strategy in cellular automata and in other spatially extended systems. This approach is based on the computational mechanics framework of Crutchfield [12], as applied to cellular automata by Crutchfield and Hanson [15, 38, 39]. This framework comprises a set of methods for classifying the different patterns that appear in CA space-time behavior, using concepts from computation and dynamical systems theories. These methods were developed as a way of analyzing the behavior of cellular automata and other dynamical systems. They extend more traditional geometric and statistical analyses by revealing the intrinsic information-processing structures embedded in dynamical processes.



(a) $\Phi_{\text{par}}^{\text{a}}$



(b) $\Phi_{\text{par}}^{\text{b}}$

Figure 6: Space-time behavior of two “particle” CAs evolved on different GA runs. (a) $\phi_{\text{par}}^{\text{a}}$ with $\rho_0 = 0.48$ (left) and $\rho_0 = 0.51$ (right). (b) $\phi_{\text{par}}^{\text{b}}$ with $\rho_0 = 0.48$ (left) and $\rho_0 = 0.51$ (right). These CAs use the boundaries between homogeneous space-time regions to effect information transmission and processing. Again, the classification of the IC is correct in each of these four cases.

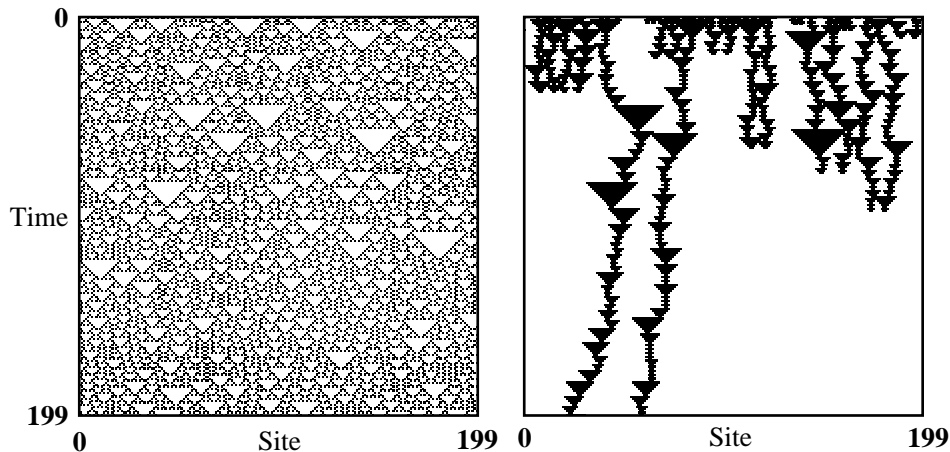


Figure 7: (a) Space-time diagram illustrating the typical behavior of ECA 18—a CA exhibiting apparently random behavior, i.e., the set of length- L spatial words has a positive entropy density as $L \rightarrow \infty$. (b) The same diagram with the regular domains—instances of words in Λ^0 —filtered out, leaving only the embedded particles $\mathbf{P} = \{1(00)^n 1, n = 0, 1, 2, \dots\}$. (After [14].)

6.1 Computational Mechanics of Cellular Automata

As applied to cellular automata, the purpose of computational mechanics is to discover an appropriate “pattern basis” with which to describe the structural components that emerge in a CA’s space-time behavior. A CA pattern basis consists of a set $\mathbf{\Lambda}$ of formal languages $\{\Lambda^i, i = 0, 1, \dots\}$ in terms of which a CA’s space-time behavior can be decomposed concisely and in a way constrained by the temporal dynamics. Once such a pattern basis is found, those cells in space-time regions that are described by the basis can be seen as forming background “domains” against which coherent structures—defects, walls, etc.—not fitting the basis move. In this way, structural features above and beyond the domains can be identified and their dynamics analyzed and interpreted on their own terms.

For example, consider the space-time diagram of Fig. 7(a), illustrating the apparently random behavior of ECA 18. This example is a useful illustration of embedded information processing since the coherent structures are not immediately apparent to the eye. The computational mechanics analysis [14, 39] of ECA 18 uses a pattern basis consisting of the single domain language $\mathbf{\Lambda} = \{\Lambda^0 = (0\Sigma)^+\}$, where $\Sigma = \{0, 1\}$. That is, over most regions in ECA 18’s configurations, every other site is a 0 and the remaining sites are wildcards, either 0 or 1. (Often this type of formal-language description of a set of configuration features can be discovered automatically via the “ ϵ -machine reconstruction” algorithm [12, 38].)

Crutchfield and Hanson define a *regular domain* Λ^j as a space-time region that (i) is a regular language and (ii) is space- and time-translation invariant. Regular domains can be represented by either the set Λ^i of configurations or by the minimal finite-state machine $M(\Lambda^i)$ that recognizes Λ^i . More specifically, let $\{\Lambda^i\}$ be the pattern basis for CA ϕ . Then the regular domain Λ^i describes the space-time regions of $\{\Phi^t(\mathbf{s}^0) : t = 0, 1, 2, \dots\}$ whose configurations are words in Λ^i . Formally, then, a regular domain Λ^i is a set that is

1. temporally invariant—the CA always maps a configuration in Λ^i to another configuration in Λ^i : $\Phi(\mathbf{s}) = \mathbf{s}'$, $\mathbf{s}, \mathbf{s}' \in \Lambda^i$; and
2. spatially homogeneous—the same pattern can occur at any site: the recurrent states in the minimal finite automaton $M(\Lambda^i)$ recognizing Λ^i are strongly connected.

Once a CA’s regular domains are discovered, either through visual inspection or by an automated induction method, and proved to satisfy the above two conditions, then the corresponding space-time regions are, in a sense, understood. Given this level of discovered regularity, the domains can be filtered out of the space-time diagram, leaving only the “unmodeled” deviations, referred to as domain “walls”, whose dynamics can then be studied in and of themselves. Sometimes, as is the case for the evolved CA we analyze here, these domain walls are spatially localized, time-invariant structures and so can be considered to be “particles”.

In ECA 18 there is only one regular domain Λ^0 . It turns out that it is stable and so is called a regular “attractor”—the stable invariant set to which configurations tend over long times, after being perturbed away from it by, for example, flipping a site value [14, 39]. Although there are random sites in the domain, its basic pattern is described by a simple rule: all configurations are allowed in which every other site value is a 0. If these fixed-value sites are on even-numbered lattice sites, then the odd-numbered lattice sites have a wild card value, being 0 or 1 with equal probability. The boundaries between these “phase-locked” regions are “defects” in the spatial periodicity of Λ^0 and, since they are spatially localized in ECA 18, they can be thought of as particles embedded in the raw configurations.

To locate a particle in a configuration generated by ECA 18, assuming one starts in a domain, one scans across the configuration, from left to right say, until the spatial period-2 phase is broken. This occurs when a site value of 1 is seen where the domain pattern indicates a 0 should be. Depending on a particle’s structure, it can occur, as it does with ECA 18, that scanning the same configuration in the opposite direction (right to left) may lead to the detection of the broken domain pattern at a different site. In this case the particle is defined to be the set of local configurations between these locations.

Due to this ECA 18’s particles are manifest in spatial configurations as blocks in the set $\mathbf{P} = \{1(00)^n1, n = 0, 1, 2, \dots\}$, a definition that is left-right scan invariant. Fig. 7(b) shows a filtered version of Fig. 7(a) in which the cells participating in Λ^0 are colored white and the cells participating in \mathbf{P} are colored black. The spatial structure of the particles is reflected in the triangular structures, which are regions of the lattice in which the particle—the breaking of Λ^0 ’s pattern—is localized, though not restricted to a single site.

In this way, ECA 18’s configurations can be decomposed into natural, “intrinsic” structures that ECA 18 itself generates; viz., its domain Λ^0 and its particle \mathbf{P} . These structures are summarized for a CA in what we call a *particle catalog*. The catalog is particularly simple for ECA 18; cf. Table 2. The net result is that ECA 18’s behavior can be redescribed at the higher level of particles. It is noteworthy that, starting from arbitrary initial configurations, ECA 18’s particles have been shown to follow a random walk in space-time on an infinite lattice, annihilating in pairs whenever they intersect [24, 39]. One consequence is that there is no further structure, such as coherent particle groupings, to understand in ECA 18’s dynamics. Thus, one moves from the deterministic dynamics at the level of the CA acting

Regular Domain
$\Lambda^0 = \{(0(0+1))^*\}$
Particle
$\alpha \sim \Lambda^0 \quad \Lambda^0 = \{1(00)^n 1, n = 0, 1, 2, \dots\}$
Interaction (annihilation)
$\alpha + \alpha \rightarrow \emptyset \quad (\Lambda^0)$

Table 2: ECA 18’s catalog of regular domains, particles, and particle interactions. The notation $p \sim \Lambda^i \Lambda^j$ means that p is the particle forming the boundary between domains Λ^i and Λ^j .

on raw configurations to a level of stochastic particle dynamics. The result is that ECA 18 configurations, such as those in Fig. 7(a), can be analyzed in a much more structural way than by simply classifying ECA 18 as “chaotic”.

In the computational mechanics view of CA dynamics, embedded particles carry various kinds of information about local regions in the IC. Given this, particle interactions are the loci at which this information is combined and processed and at which decisions are made. In general, these structural aspects—domains, particles, and interactions—do not appear immediately. As will be seen below, often there is a initial disordered period, after which the configurations condense into well-defined regular domains, particles, and interactions. To capture this relaxation process we define the *condensation time* t_c as the first iteration at which the filtered space-time diagram contains only well-defined domains in $\mathbf{\Lambda}$ and the walls between them. In other words, at t_c , every cell participates in either a regular domain, of width at least $2r + 1$, in a wall between them, or in an interaction between walls. (See Refs. [16] and [42] for a more detailed discussion of the condensation phase and its consequences.)

6.2 Computational Mechanics of Evolved Cellular Automata

This same methodology is particularly useful in understanding and formalizing the computational strategies that emerged in the GA-evolved CA. Fortunately, in the following exposition most of the structural features in the evolved CA are apparent to the eye. Fig. 6(a) suggests that an appropriate pattern basis for $\phi_{\text{par}}^{\text{a}}$ is $\mathbf{\Lambda} = \{\Lambda^0 = 00^+, \Lambda^1 = 11^+, \Lambda^2 = (01)^+\}$, corresponding to the all-white, all-black, and checkerboard regions. Similarly, Fig. 6(b) suggests that for $\phi_{\text{par}}^{\text{b}}$ we use $\mathbf{\Lambda} = \{\Lambda^0 = 00^+, \Lambda^1 = 111^+, \Lambda^2 = (011)^+\}$, corresponding to the all-white, all-black, and striped regions.

Note that a simple shortcut can be used to identify domains that are spatially and temporally periodic. If the same “pattern” appears repeated over a sufficiently large ($\gg r$ cells by r time steps) space-time region, then it is a domain. It is also particularly easy to prove such regions are regular domains. Exactly how the pattern is expressed as a regular language or as a minimal finite-state machine typically requires closer inspection.

Once identified, the computational contributions of these space-time regions can be easily understood. The contributions consist solely of the generation of words in the cor-

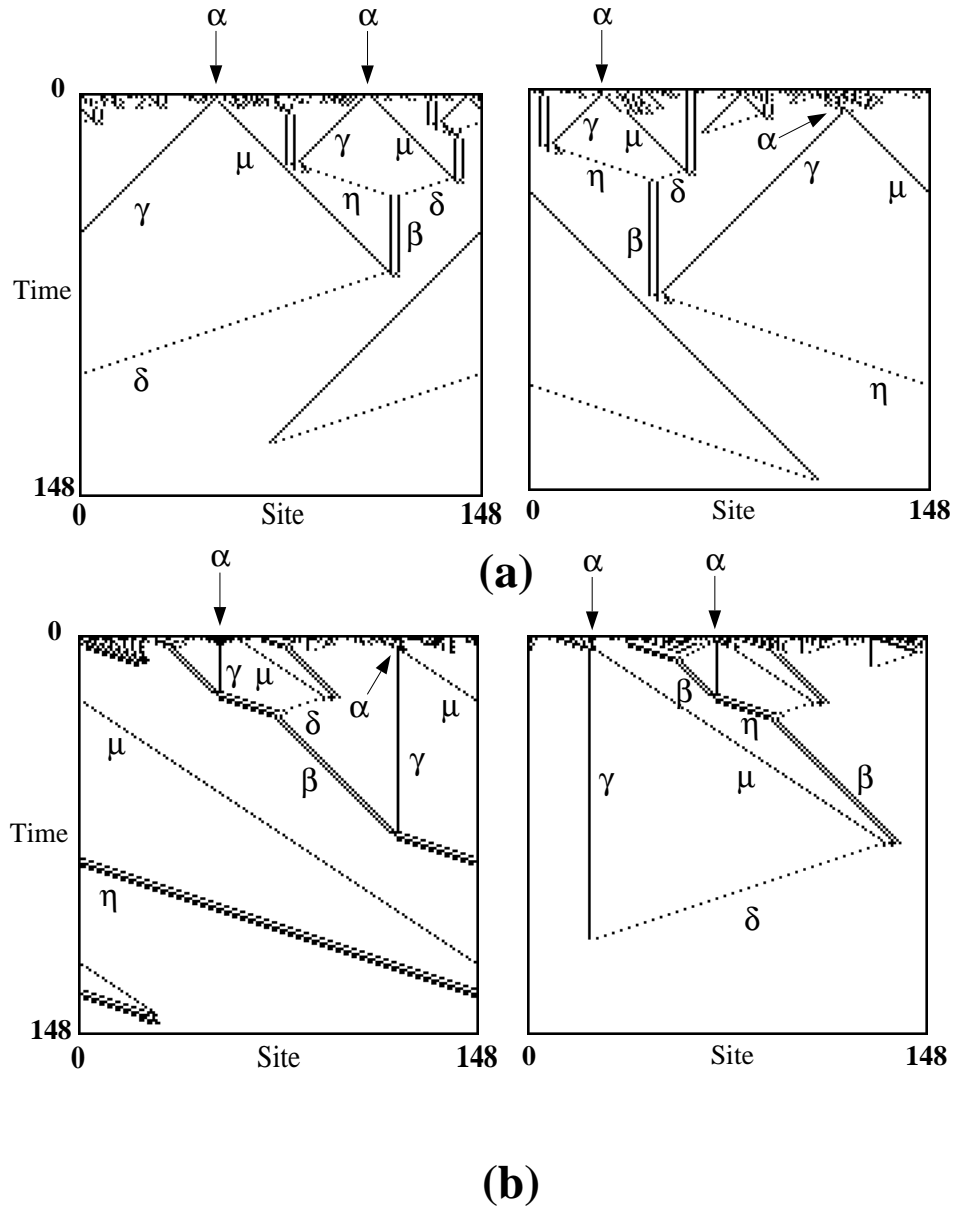


Figure 8: (a) Version of Fig. 6(a) with the regular domains filtered out, revealing the particles and their interactions. (b) Filtered version of Fig. 6(b).

Regular Domains		
$\Lambda^0 = \{0^+\}$	$\Lambda^1 = \{1^+\}$	$\Lambda^2 = \{(01)^+\}$
Particles (Velocities)		
$\alpha \sim \Lambda^0 \Lambda^1 (-)$	$\beta \sim \Lambda^1 \Lambda^0 (0)$	$\gamma \sim \Lambda^0 \Lambda^2 (-1)$
$\delta \sim \Lambda^2 \Lambda^0 (-3)$	$\eta \sim \Lambda^1 \Lambda^2 (3)$	$\mu \sim \Lambda^2 \Lambda^1 (1)$
Interactions		
decay	$\alpha \rightarrow \gamma + \mu$	
react	$\beta + \gamma \rightarrow \eta, \mu + \beta \rightarrow \delta, \eta + \delta \rightarrow \beta$	
annihilate	$\eta + \mu \rightarrow \emptyset (\Lambda^1), \gamma + \delta \rightarrow \emptyset (\Lambda^0)$	

Table 3: $\phi_{\text{par}}^{\text{a}}$'s catalog of regular domains, particles (including velocities in parentheses), and particle interactions. Note that this catalog leaves out possible three-particle interactions.

responding regular language. Since this requires only a finite amount of spatially localized memory, its direct contribution to the global computation required by the task is minimal. (The density of memory vanishes as the domain increases in size.) The conclusion is that the domains themselves, while necessary, are not the locus of the global information processing.

Fig. 8 is a version of Fig. 6 with $\phi_{\text{par}}^{\text{a}}$'s and $\phi_{\text{par}}^{\text{b}}$'s regular domains filtered out. The result reveals the walls between them, which for $\phi_{\text{par}}^{\text{a}}$ and $\phi_{\text{par}}^{\text{b}}$ are several kinds of embedded particles. The particles in Fig. 8 are labeled with Greek letters. This filtering is performed by a building a transducer that reads in the raw configurations and can recognize when sites are in which domain. The transducer used for Fig. 8(a), for example, outputs white at each site in one of $\phi_{\text{par}}^{\text{a}}$'s domains and black at each site participating in a domain wall. (The particular transducer and comments on its construction and properties can be found in Appendix A. The general construction procedure is given in Ref. [15].)

Having performed the filtering, the focus of analysis shifts away from the raw configurations to the new level of embedded-particle structure. The questions now become, Are the computational strategies explainable in terms of particles and their interactions? Or, is there as yet some unrevealed information processing occurring that is responsible for high performance?

Tables 3 and 4 list all the different particles that are observed in the space-time behavior of $\phi_{\text{par}}^{\text{a}}$ and $\phi_{\text{par}}^{\text{b}}$, along with their velocities and the interactions that can take place between them. Note that these particle catalogs do not include all possible structures, for example, possible three-particle interactions. The computational strategies of $\phi_{\text{par}}^{\text{a}}$ and $\phi_{\text{par}}^{\text{b}}$ can now be analyzed in terms of the particles and their interactions as listed in the particle catalogs.

6.3 Computational Strategy of $\phi_{\text{par}}^{\text{a}}$

In a high-performance CA such as $\phi_{\text{par}}^{\text{a}}$, particles carry information about the density of local regions in the IC, and their interactions combine and process this information, rendering a series of decisions about ρ_0 . How do these presumed “functional” components lead to the

Regular Domains		
$\Lambda^0 = \{0^+\}$	$\Lambda^1 = \{1^+\}$	$\Lambda^2 = \{(011)^+\}$
Particles (Velocities)		
$\alpha \sim \Lambda^1 \Lambda^0 (0)$	$\beta \sim \Lambda^0 \Lambda^1 (1)$	$\gamma \sim \Lambda^1 \Lambda^2 (0)$
$\delta \sim \Lambda^2 \Lambda^1 (-3)$	$\eta \sim \Lambda^0 \Lambda^2 (3)$	$\mu \sim \Lambda^2 \Lambda^0 (3/2)$
Interactions		
decay	$\alpha \rightarrow \gamma + \mu$	
react	$\beta + \gamma \rightarrow \eta, \mu + \beta \rightarrow \delta, \eta + \delta \rightarrow \beta$	
annihilate	$\eta + \mu \rightarrow \emptyset (\Lambda^0), \gamma + \delta \rightarrow \emptyset (\Lambda^1)$	

Table 4: $\phi_{\text{par}}^{\text{b}}$'s catalog of regular domains, particles (including their velocities in parentheses), and particle interactions.

observed fitness and computation performance?

Referring to Table 3 and Fig. 8(a), $\phi_{\text{par}}^{\text{a}}$'s β particle is seen to consist of the zero-velocity black-to-white boundary. β carries the information that it came from a region in the IC in which the density is locally ambiguous: the density of $1^k 0^k$, when determined at its center, is exactly ρ_c . The ambiguity cannot be resolved locally. It might be, however, at a later time, when more information can be integrated from other regions of the IC.

Likewise, the α “particle” consists of the white-to-black boundary, but unlike the β particle, α is unstable and immediately decays into two particles γ (white-checkerboard boundary) and μ (checkerboard-black boundary). Like β , α indicates local density ambiguity. The particles into which it decays, γ and μ , carry this information and so they too are “ambiguous density” signals. γ carries the information that it borders a white (low density) region and μ carries the information that it borders a black (high density) region. The two particles also carry the mutual information of having come from the same ambiguous density region where the transient α was originally located. They carry this positional information about α 's location by virtue of having the same speed (± 1).

To see how these elements work together over a space-time region consider the left side of the left-hand ($\rho_0 < 1/2$) diagram in Fig. 8(a). Here, α decays into a γ and a μ particle. The μ then collides with a β before its companion γ (wrapping around the lattice) does. This indicates that the low-density white region, whose right border is the γ , is larger than the black region bordered by the μ . The μ - β collision creates a new particle, a δ , that carries this information (“low-density domains”) to the left, producing more low-density area. δ , a fast moving particle, catches up with the γ (“low density”) and annihilates it, producing Λ^0 over the entire lattice. The result is that the white region takes over the lattice before the maximum number of iterations has passed. In this way, the classification of the (low density) IC has been correctly determined by the spatial algorithm—the steps we have just described. In the case of $\phi_{\text{par}}^{\text{a}}$, this final decision is implemented by δ 's velocity being three times that of γ 's.

On the right side of the right-hand ($\rho_0 > 1/2$) diagram in Fig. 8(a), a converse situation emerges: γ collides with β before μ does. The effective decision indicates that the black

region bordered by μ is larger than the white region bordered by γ . In symmetry with the μ - β interaction described above, the γ - β interaction creates the η particle that catches up with the μ and the two annihilate. In this way, the larger black region takes over and the correct density classification is effected.

A third type of particle-based information processing is illustrated at the top left of the right-hand diagram in Fig. 8(a). Here, an α decays into a γ and a μ . In this case, the white region bordered by γ is smaller than the black region bordered by μ . As before, γ collides with the β on its left, producing η . However, there is another β particle to the right of μ . Instead of the μ proceeding on to eventually collide with the η , the μ first collides with the second β . Since the μ borders the larger of the two competing regions, its collision is slightly later than the γ - β collision to its left. The μ - β collision produces a δ particle propagating to the left. Now the η and the δ approach each other at equal and opposite speeds and collide. Since η is carrying the information that the white region should win and δ is carrying the information that the black region should win, their collision appropriately results in an “ambiguity” signal—here, a β that later on interacts with particles from greater distances. But since η traveled farther than δ before their collision, a β is produced that is shifted to the right from the original α . The net effect—the net geometric subroutine—is to shift the location of density ambiguity from that of the original α particle in the IC to a β moved to the right a distance proportional to the large black region’s size relative to the white region’s size.

Even though this β encodes ambiguity that cannot be resolved by the information currently at hand—that is, the information carried by the η and δ that produce it—this β actually carries important information in its location, which is shifted to the right from the original α . To see this, refer to Fig. 9, an enlargement of the right diagram of Fig. 8(a) with some particle labels omitted for clarity. \mathbf{W} and \mathbf{B} denote the lengths of the indicated white (low density) and black (high density) regions in the IC. Given the particle velocities listed in Table 3 and using simple geometry it is easy to calculate that the β , produced by the η - δ interaction, is shifted to the right by $2(\mathbf{B} - \mathbf{W})$ cells from the α ’s original position. The shift to the right means that the high-density region (to the left of the leftmost β) has gained $\mathbf{B} - \mathbf{W}$ sites in size as a result of this series of interactions. In terms of relative position the local particle configuration $\beta\alpha\beta$ becomes $\beta\gamma\mu\beta$ and then $\eta\delta$, which annihilate to produce a final β . This information is used later on, when the rightmost γ collides with the new β before its partner μ does, eventually leading to black taking over the lattice, correctly classifying the ($\rho_0 > 1/2$) IC.

It should now be clear in what sense we say that particles store and transmit information and that particle collisions are the loci of decision making. We described in detail only two such scenarios. As can be seen from the figures, this type of particle-based information processing occurs in a distributed, parallel fashion over a wide range of spatial and temporal scales. The functional organization of the information processing can be usefully analyzed at three levels: (i) the information stored in the particles and decisions made during their interaction, (ii) geometric subroutines that are coordinated groupings of particles and interactions that effect intermediate-scale functions, and (iii) the net spatial computation over the whole lattice and from $t = 0$ to $t = T_{\max}$.

In the next section we will argue that these levels of description of a CA’s computational behavior—in terms of information transmission and processing by particles and

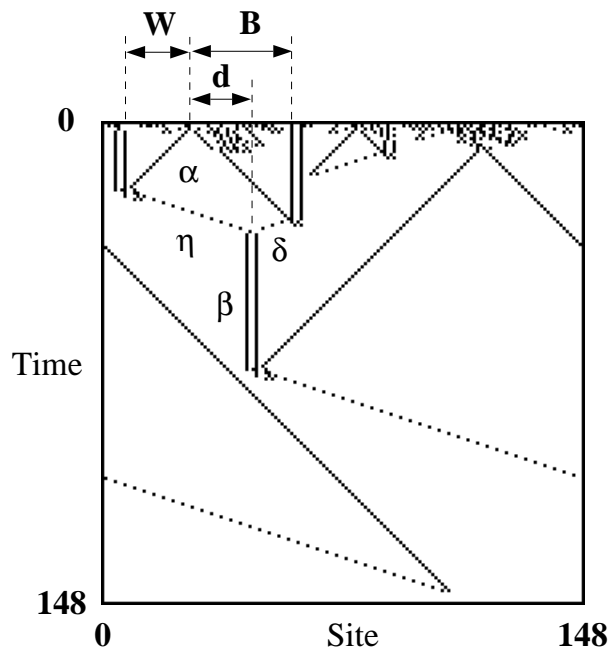


Figure 9: An enlargement and relabeling of the right diagram of Fig. 8(a) with some particle labels omitted for clarity. \mathbf{W} is the length of the leftmost white region, \mathbf{B} is the length of the black region to its right, and \mathbf{d} is the amount by which the β produced by the η - δ interaction has been shifted from the leftmost α . Given the particle velocities listed in Table 3 and using simply geometry, it is easy to calculate that $\mathbf{d} = 2(\mathbf{B} - \mathbf{W})$.

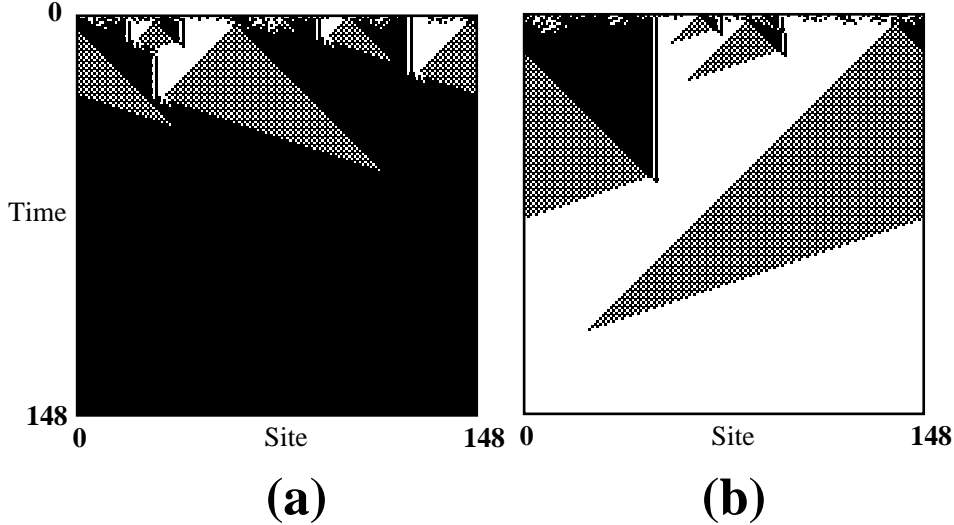


Figure 10: (a) Type-1 misclassification by $\phi_{\text{par}}^{\text{a}}$, with $\rho_0 = 0.48$. Even though $\rho_0 < \rho_c$, at t_c (here, $t = 8$) the lengths of the black regions sum to 65 cells and the lengths of the white regions sum to 44 cells. This leads to a misclassification of IC density. (b) Type-2 misclassification by $\phi_{\text{par}}^{\text{a}}$, starting with $\rho_0 = 0.52$. At t_c (here also, $t = 8$) the sum of the lengths of the black regions is 65 cells and the sum of the lengths of the white regions is 61 cells. However, even though these condensed lengths correctly reflect the fact that $\rho_0 > \rho_c$, the black regions in the IC's center occur within white regions in such a way that they get cut off. Ultimately this yields a large white region that wins over the large black region and the IC is misclassified.

their interactions—is analogous to, but significantly extends, Marr’s “representation and algorithm” level of information processing. It turns out to be the most useful level for understanding and predicting the computational behavior of CAs, both for an individual CA operating on particular ICs and also for understanding how the GA evolved the progressive innovations in computational strategies over succeeding generations. (We will put these latter claims on a quantitative basis shortly.)

$\phi_{\text{par}}^{\text{a}}$ almost always iterates to either all 0s or all 1s within $T_{\text{max}} = 2N$ time steps. The errors it makes are almost always due to the wrong classification being reached rather than no classification being effected. $\phi_{\text{par}}^{\text{a}}$ makes two types of misclassifications. In the first type, illustrated in Fig. 10(a), $\phi_{\text{par}}^{\text{a}}$ reaches the condensation time t_c having produced a configuration whose density is on the opposite side of ρ_c than was ρ_0 . The particles and interactions then lead, via a correct geometric computation, to an incorrect final configuration. In the second type of error, illustrated in Fig. 10(b), the density ρ_{t_c} is on the same side of the threshold as ρ_0 , but the configuration is such that islands of black (or white) cells are isolated from other black (or white) regions and get cut off. This error in the geometric computation eventually leads to an incorrect final configuration. As N increases, this type of error becomes increasingly frequent and results in the decreasing $\mathcal{P}_N^{10^4}$ values at larger N ; see Table 1.

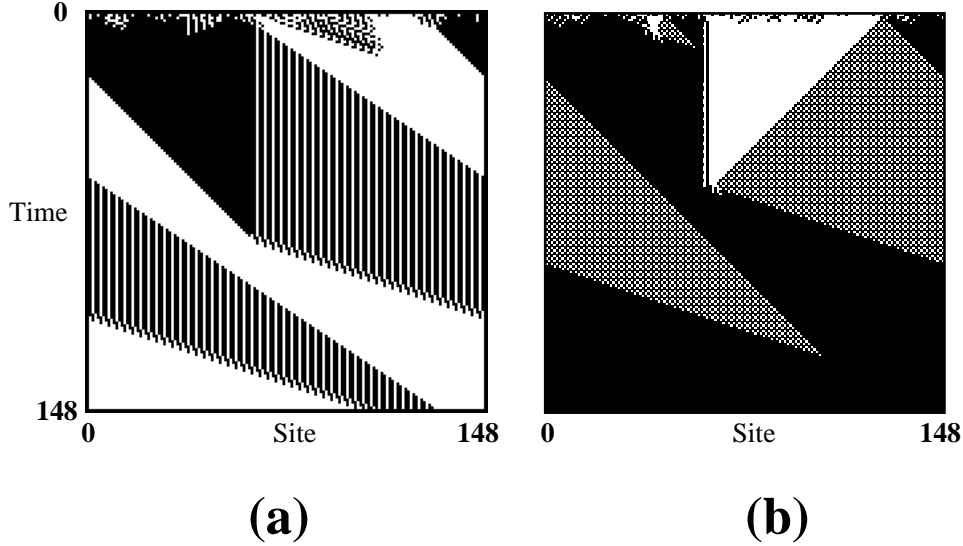


Figure 11: (a) Misclassification by $\phi_{\text{par}}^{\text{b}}$, with $\rho_0 = 0.52$. (By $T_{\text{max}} = 2N$, the CA reaches an all-0s fixed point.) (b) Correct classification by $\phi_{\text{par}}^{\text{a}}$ on the same IC.

6.4 Computational Strategy of $\phi_{\text{par}}^{\text{b}}$ —Failure Analysis

As noted in Table 4, the space-time behavior of $\phi_{\text{par}}^{\text{b}}$ exhibits three regular domains: Λ^0 (white), Λ^1 (black), and Λ^2 (striped). The size-competition strategy of $\phi_{\text{par}}^{\text{b}}$ is similar to that of $\phi_{\text{par}}^{\text{a}}$. In $\phi_{\text{par}}^{\text{b}}$, the striped region plays the role of $\phi_{\text{par}}^{\text{a}}$'s checkerboard domain. However, when compared to $\phi_{\text{par}}^{\text{a}}$, the roles of the two domain boundaries $\Lambda^0\Lambda^1$ and $\Lambda^1\Lambda^0$ are now reversed. In $\phi_{\text{par}}^{\text{b}}$, $\Lambda^0\Lambda^1$ is stable, while $\Lambda^1\Lambda^0$ is unstable and decays into two particles. Thus, the strategy used by $\phi_{\text{par}}^{\text{b}}$ is, roughly speaking, a 0-1 site-value exchange applied to $\phi_{\text{par}}^{\text{a}}$'s strategy. Particles α , β , γ , δ , η , and μ are all analogous in the two CAs, as are their interactions, if we exclude three-particle interactions; cf. Tables 3 and 4. They implement competition between adjacent large white and black regions. In analogy with the preceding analysis for $\phi_{\text{par}}^{\text{a}}$'s strategy, these local competitions are decided by which particle, a γ or a μ , reaches a β first.

In $\phi_{\text{par}}^{\text{a}}$, γ and μ each approach β at the rate of one cell per time step. In $\phi_{\text{par}}^{\text{b}}$, although γ is now a stationary particle, it also effectively approaches β at the rate of 1 cell per time step, since β moves with velocity 1. μ approaches β at the rate of 1/2 cell per time step, the velocity of μ minus the velocity of β . Thus, there is an asymmetry in $\phi_{\text{par}}^{\text{b}}$'s geometric computation that can result in errors of the type illustrated in Fig. 11(a). There the IC, with $\rho = 0.52$, condenses around iteration $t_c \approx 20$ into a block of 85 black cells adjacent to a block of 64 white cells. The γ particle, traveling at velocity 1 relative to β , reaches β in approximately 85 time steps. The μ particle, traveling at velocity 1/2 relative to β , reaches β in approximately 103 time steps. Thus, even though the black cells initially outnumber the white cells, the black region is cut off first and white eventually wins out, yielding an incorrect classification at time step 165. In contrast, $\phi_{\text{par}}^{\text{a}}$, with its symmetric particle

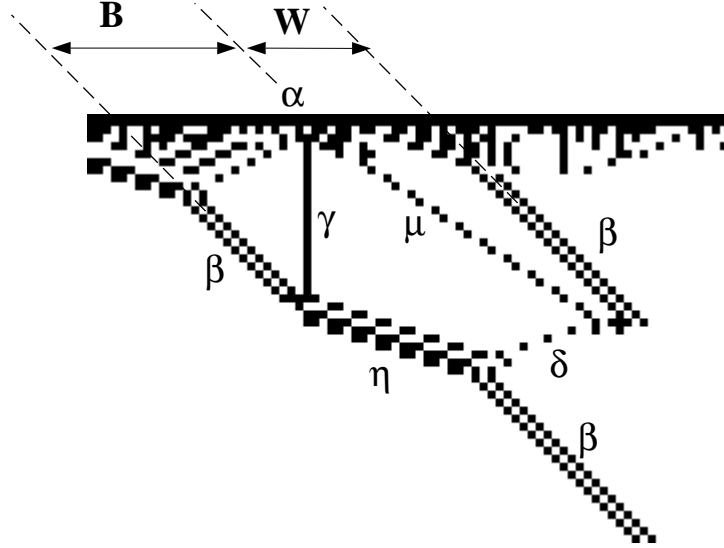


Figure 12: Blow-up of part of right-hand diagram of Fig. 8b, illustrating asymmetries in $\phi_{\text{par}}^{\text{b}}$'s particle velocities that can result in misclassifications.

velocities, reaches a correct classification on this same IC (Fig. 11(b)).

Like $\phi_{\text{par}}^{\text{a}}$, $\phi_{\text{par}}^{\text{b}}$ makes two types of classification errors—the type in which $\phi_{\text{par}}^{\text{b}}$ reaches t_c with a configuration whose density ρ_{t_c} is on the opposite side of ρ_c than ρ_0 and the type illustrated in Fig. 11(a). The first type (“type 1”) is an error in how the CA condenses into domains and particles. The second type (“type 2”) is due to asymmetries in particle velocities. Consider Fig. 12, a blow-up of part of the right-hand diagram of Fig. 8(b). To the left of the α (labeled) is an isolated black island and to the right is a white island. Together these two contiguous islands are bounded by two β particles on either side. Inside, as in $\phi_{\text{par}}^{\text{a}}$, an α decays into a γ and a μ . The resulting set of local particle interactions is such that the two islands compete for space within the two bounding β 's, ending with the creation of a new β . If \mathbf{W} and \mathbf{B} respectively denote the lengths of the white and black islands, then after a series of interactions— $\beta\gamma\mu\beta \rightarrow \eta\delta \rightarrow \beta$ —the white region (to the left of the original leftmost β) gains $2\mathbf{W} - \mathbf{B}$ sites in size. Thus, to increase this region's size the internal white island must be at least half the size of its adjacent black island.

It is evident, therefore, that unlike $\phi_{\text{par}}^{\text{a}}$, there are asymmetries in $\phi_{\text{par}}^{\text{b}}$'s particle “logic”, and these are biased in favor of classifying high densities. These asymmetries are what make $\mathcal{P}_N^{10^4}(\phi_{\text{par}}^{\text{b}})$ lower than $\mathcal{P}_N^{10^4}(\phi_{\text{par}}^{\text{a}})$. (See Table 1.)

7. Significance of the Particle-Level Description

There are several alternative ways in which cellular automata such as $\phi_{\text{par}}^{\text{a}}$ and $\phi_{\text{par}}^{\text{b}}$ can be described as performing a computation. Marr anticipated some of these in delineating the various levels of information processing in vision [51]. In principle, our CAs are completely described by the 128 bits in their look-up tables. This is too low-level a description, however, to be useful for understanding how a given CA performs the $\rho_c = 1/2$ task. Using this level

is like trying to understand how a pocket calculator computes the square root function by examining the physical equations of motion for the electrons and holes in the calculator’s silicon circuitry.

Moreover, attempting interpretation at this level also violates, in a sense, one of the central tenets of the century-long study of dynamical systems, namely, that for nonlinear systems (e.g., most CAs), the local space-time equations of motion do not *directly* determine the system’s long-term behavior. In the case of CAs it is not the individual look-up table neighborhood-output-bit entries acting over a single time step that directly give rise to the observed computational strategy. Instead, it is the interaction of *subsets* of CA look-up table entries that over a *number of iterations* leads to the emergence of domains, particles, and interactions.

A second possibility for describing computational behavior in CAs is in terms of its detailed space-time behavior—i.e., the series of raw configurations of 0s and 1s. Again, this description is too low level for understanding how the solutions to the task are implemented. This approach is like trying to understand how a calculator’s square root function is performed by taking a long series snapshots of the positions and velocities of the electrons and holes traveling through the integrated circuits. This prosaic view is analogous to Marr’s “hardware implementation” level of description [51].

A third possibility is to describe the CA in terms related to the task’s required input/output mapping and the task’s computational complexity. For example, on a particular set of 10^4 random ICs, half with $\rho < 1/2$ and half with $\rho > 1/2$, $\phi_{\text{par}}^{\text{a}}$ correctly classified 81% of the $\rho < 1/2$ ICs and 74% of the $\rho > 1/2$ ICs. On average $\phi_{\text{par}}^{\text{a}}$ took 81 time steps to reach a fixed point; the maximum time was 227. The computational complexity of the $\rho_c = 1/2$ task on a serial architecture is $\mathcal{O}(N)$. This kind of operational analysis is roughly at Marr’s “computational theory” level.

None of these levels of description gives much insight into *how* the task is being performed by a particular CA in terms of what information processing is being done and how it leads to a particular measured performance. What is needed is an intermediate-level description whose primitives are informationally related to the task at hand. This is what the computational mechanics level of particles and particle interactions gives us. How ever one might detect the primitives at this level, it is analogous to Marr’s “representation and algorithm” level, in which particles can be seen as representing aspects of the IC and their actions and interactions can be seen as the CA’s emergent algorithm.

Representations, in the form of data structures, and algorithms have been studied extensively for von Neumann-style computers, but there have been few attempts to define such notions for decentralized spatially extended systems such as CAs. One can, of course, in principle implement any standard data structure and algorithm in a computation-universal CA, such as the game of Life CA [3], by simulating a von Neumann-style computer. However, this is not a particularly useful notion of information processing if one’s goals are to understand how nonlinear systems in nature compute. It is even more problematic if one wishes to design computation in complex decentralized spatially extended architectures. We believe that it will be essential to develop new “macroscopic-level” vocabularies in order to explain how collective information processing takes place in such architectures. (One benefit of this development would be an understanding of how to program these architectures in

genuinely parallel ways.)

A close reading shows that Marr’s analysis of the descriptive levels required for visual processing misses several key issues. These are (i) the fact that representations emerge from the dynamics (i.e., are *intrinsic* to the dynamics), (ii) a clear formal definition is required to remove the subjectivity of detecting these intrinsic representations, and (iii) their functionality is entailed by a new level of dynamics, also intrinsic, that describes their interactions. As illustrated above in several cases, the computational mechanics framework that we are employing here makes these distinctions and provides the necessary concepts and methods to address these issues [12, 13]. The result is that we can analyze in detail the emergent computational strategies in the evolved CAs.

Our particle-level description forms an explanatory vocabulary for emergent computation in the context of one-dimensional, binary-state CAs. As was described above, particles represent various kinds of information about the IC and particle interactions are the loci of decision making that use this information. The resulting particle “logic” gives a functional description of how the computation takes place that is neither directly available from the CA look-up table nor from the raw space-time configurations produced by iterating the CA. It gives us a formal notion of “strategy”, allowing us to see, for example, how the strategies of ϕ_{par}^a and ϕ_{par}^b are similar and how they differ. One immediate consequence of this level of analysis is that we can say why ϕ_{par}^b ’s strategy is weaker.

The level of particles and interactions is not only a qualitative description of spatial information processing, it also enables us to make quantitative predictions about computational performance. In Refs. [16] and [42], we describe how to model a CA using its particle catalog and statistical properties at the condensation time. For each of several different CAs ϕ , we compare the model’s prediction for $\mathcal{P}_N^I(\phi)$ as well as for the average time taken to reach a fixed point with the values measured for the actual ϕ . Some of these comparisons will be summarized in Sec. 8.7. The degree to which a model’s predictions agree with the corresponding CA’s behavior indicates the degree to which the particle-level description captures how the CA is actually performing the computation. Since, as we will show, the model’s predicted performance and the observed performance are very close, we conclude that the particle-level description accurately captures the intrinsic computational capability of the evolved CAs.

8. Evolutionary History of ϕ_{par}^a : Innovation, Contingency, and Exaptation

The structural analysis of CA space-time information processing that we have just outlined also allows us to understand the evolutionary stages during which the GA produces CAs. Here we will show how the functional components—domains, particles, and interactions—arise and are inherited across the evolutionary history of a GA run. We will also demonstrate a number of evolutionary dynamical phenomena, such as the historical contingency of functional emergence and the appearance of initially nonfunctional behaviors that later are key to the final appearance of high performance CAs.

To begin, Figures 13(a) and 13(b) illustrate ϕ_{par}^a ’s evolutionary history. Fig. 13(a) gives a partial tree of the parent-child relationships between some of ϕ_{par}^a ’s ancestors, each numbered by its generation of birth. Note that, since elite CAs can survive for more than

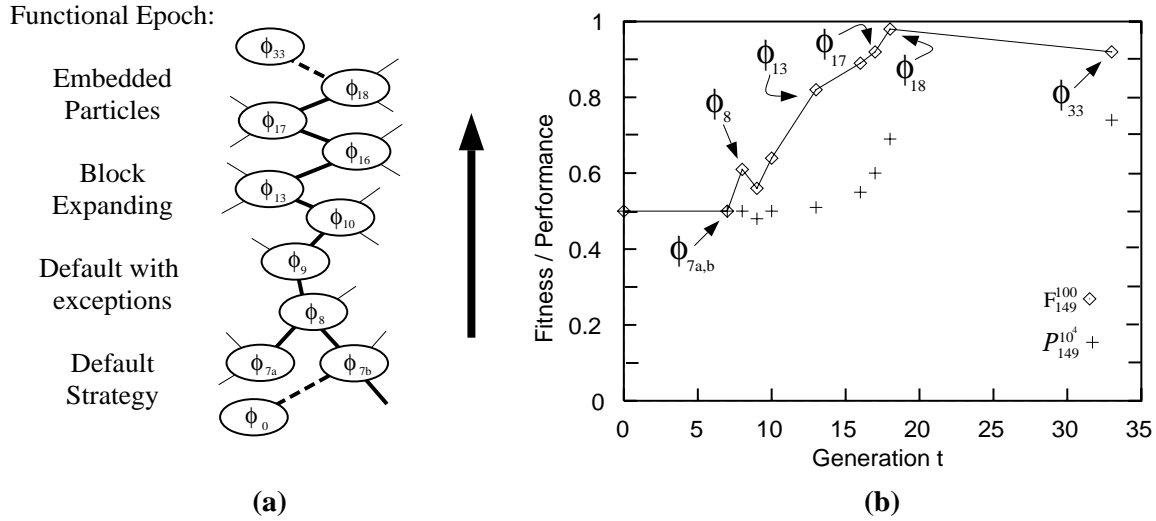


Figure 13: (a) Partial ancestral tree of $\phi_{\text{par}}^{\text{a}}$. (b) $F_{149}^{100}(\phi)$ (diamonds) and $\mathcal{P}_{149}^{10^4}(\phi)$ (crosses) of the CAs ϕ_i in (a). Six of the data points are marked with the name of the corresponding CA.

CA Name	Rule Table (Hexadecimal)	F_{149}^{100}	$\mathcal{P}_{149}^{10^4}$
ϕ_{7b}	F6EFFFFFFFFFFFFFFF 6B9F7F93FFFFFFBFFF	0.50	0.500
ϕ_8	0400448102000FFF 6B9F7F93FFFFFFBFFF	0.61	0.500
ϕ_{13}	0400458100000FFF 6B9F77937DFFFFFF7F	0.82	0.513
ϕ_{17}	0500458100000FBF 6B9F75937FBFFF5F	0.92	0.595
ϕ_{18}	0500458100000FBF 6B9F75937FBDF77F	0.98	0.691
ϕ_{33}	0504058100840FB7 4BBF55837FBDF77F	0.97	0.735

Table 5: CA chromosomes (look-up table output bits) given in hexadecimal, F_{149}^{100} , and $\mathcal{P}_{149}^{10^4}$ for the six ancestors of $\phi_{\text{par}}^{\text{a}}$ described in this section. (See Fig. 1 for directions on how to recover the CA rule table outputs from the hexadecimal code.) The F_{149}^{100} values in this table are those calculated in the CA's generation of birth by the GA; the $\mathcal{P}_{149}^{10^4}$ values given are the means over 100 trials of the performance function, calculated after the run was complete. When tested over 100 trials, the standard deviation of F_{149}^{100} is approximately 0.02 and the standard deviation of $\mathcal{P}_{149}^{10^4}$ is approximately 0.005 for each CA.

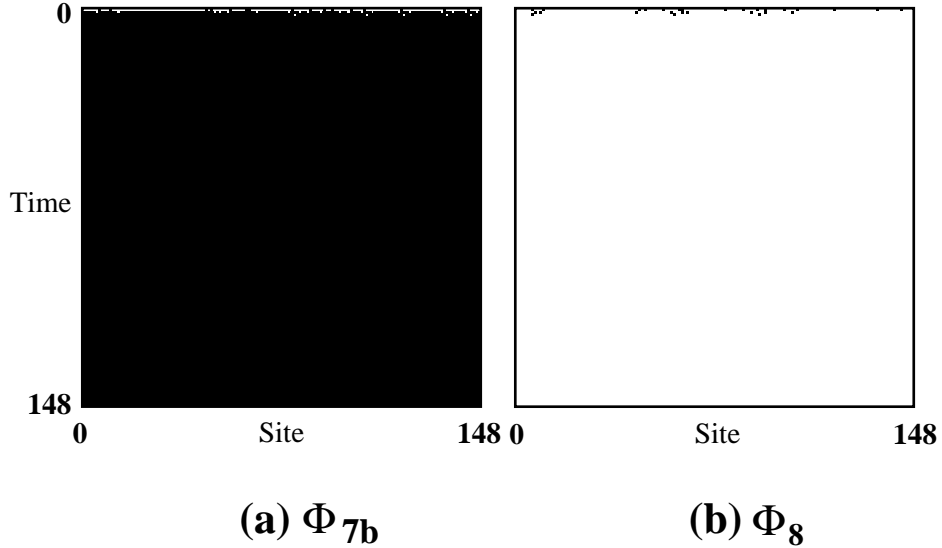


Figure 14: Space-time behavior of generation 7 and 8 ancestors, ϕ_{7b} and ϕ_8 , of ϕ_{par}^a . Both start from the same IC with $\rho_0 = 0.11$.

one generation, parents and offspring, e.g. ϕ_{10} and ϕ_{13} , can have nonconsecutive generation labels. The CAs listed are those with the best fitness in the generation in which they arose. Table 5 lists the look-up tables, F_{149}^{100} , and $\mathcal{P}_{149}^{10^4}$ for the six ancestors of ϕ_{par}^a described below.

Fig. 13(b) plots F_{149}^{100} (diamonds) and $\mathcal{P}_{149}^{10^4}$ (crosses) versus generation of birth for each of these ancestors. In generations 0–7 the best CA in the population has $F_{149}^{100} = \mathcal{P}_{149}^{10^4} = 0.5$, achieved by a “default” strategy like those of Fig. 4. Starting at generation 8, evolution proceeds in a series of abrupt increases in F_{149}^{100} . More gradual increases are seen in $\mathcal{P}_{149}^{10^4}$; of course, this statistic is not available to and thus is not used by the GA. The occasional small decreases result from the stochastic nature of the fitness and performance evaluations.

The goal now is to use the functional analysis to understand why these increases come about. To do so, we present a series of space-time diagrams, in Figs. 14-19, that compare space-time behaviors of CAs along the ancestral tree of Fig. 13(a). In each figure, space-time behavior with the same IC is given for two ancestrally related CAs to highlight the similarities and evolutionary innovations.

8.1 ϕ_{7b} and ϕ_8 (Fig. 14)

Here the IC has very low density: $\rho_0 = 0.11$. ϕ_{7b} , a “default” CA, always iterates to all 1s, and in Fig. 14(a) misclassifies the IC. ϕ_{7a} (not shown) is a default CA that always iterates to all 0s. ϕ_{7b} ’s look-up table contains mostly 1s (see Table 5) and ϕ_{7a} ’s look-up table contains mostly 0s. They crossed over at locus 52 to produce ϕ_8 : therefore the first part of ϕ_8 ’s look-up table contains mostly 0s, and the rest is mostly 1s. In Fig. 14(b) ϕ_8 iterates to all 0s and correctly classifies the IC.

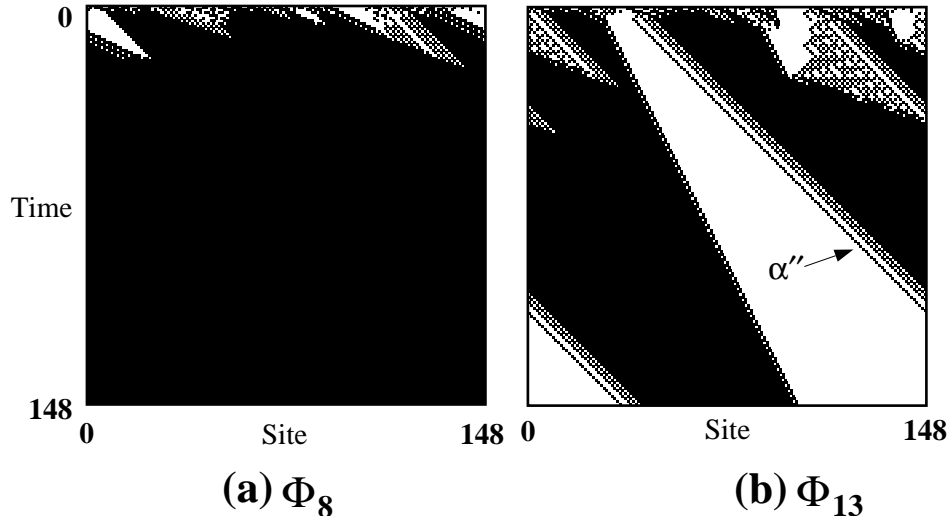


Figure 15: Space-time behavior of generation 8 and 13 ancestors, ϕ_8 and ϕ_{13} , of $\phi_{\text{par}}^{\text{a}}$. Both start from the same IC with $\rho_0 = 0.47$. (The significance of α'' is explained below, when ϕ_{13} and ϕ_{17} are compared.)

8.2 ϕ_8 and ϕ_{13} (Fig. 15)

Here $\rho_0 = 0.47$. In Fig. 15(a) ϕ_8 quickly iterates to all 1s. This is its more typical behavior than that shown in Fig. 14(b); very small regions of black quickly grow to take over the entire lattice. In this way, ϕ_8 is only slightly better than a default CA like ϕ_{7b} ; it correctly classifies all high-density ICs and only a small number of very low density ICs. Note that while $F_{149}^{100}(\phi_8) > 0.5$, $\mathcal{P}_{149}^{10^4}(\phi_8)$ remains at 0.5. ϕ_8 can be said to be carrying out a “default-with-exceptions” strategy. All runs that produced such strategies went on to converge on either block-expanding strategies or embedded-particle strategies.

Interestingly, the checkerboard domain $\Lambda^2 = \{(01)^+\}$ is produced by ϕ_8 on some ICs (Fig. 15). However, Λ^2 does not contribute to ϕ_8 ’s fitness or performance. It is a functionally neutral feature. To determine this, we modified ϕ_8 ’s rule table to prevent the checkerboard domain from propagating. The two relevant entries are $0101010 \rightarrow 0$ and $1010101 \rightarrow 1$. Flipping the output bit on either or both of these entries produces CAs with $F_{149}^{100} = 0.61$ and $\mathcal{P}_{149}^{10^4} = 0.5$; that is, fitness and performance identical to those of ϕ_8 . (The standard deviations of F_{149}^{100} for this and the other variant CAs discussed in this section were approximately 0.02. The standard deviations of $\mathcal{P}_{149}^{10^4}$ were approximately 0.005.) Appropriating biological terminology, we can consider the checkerboard domain, at this generation, to be an adaptively neutral trait of ϕ_8 .

ϕ_{13} represents a steep jump in fitness over ϕ_8 , as seen in Fig. 13(b). ϕ_{13} is a block-expanding CA. It maps ICs to all 1s unless there is a sufficiently large block of adjacent 0s in the IC, in which case that block expands to eventually fill up the entire lattice, as in Fig. 15(b), which is a correct classification by $t = T_{\text{max}}$. On some ICs, ϕ_{13} also produces a checkerboard domain and a similar but less ordered region; the latter can be seen in

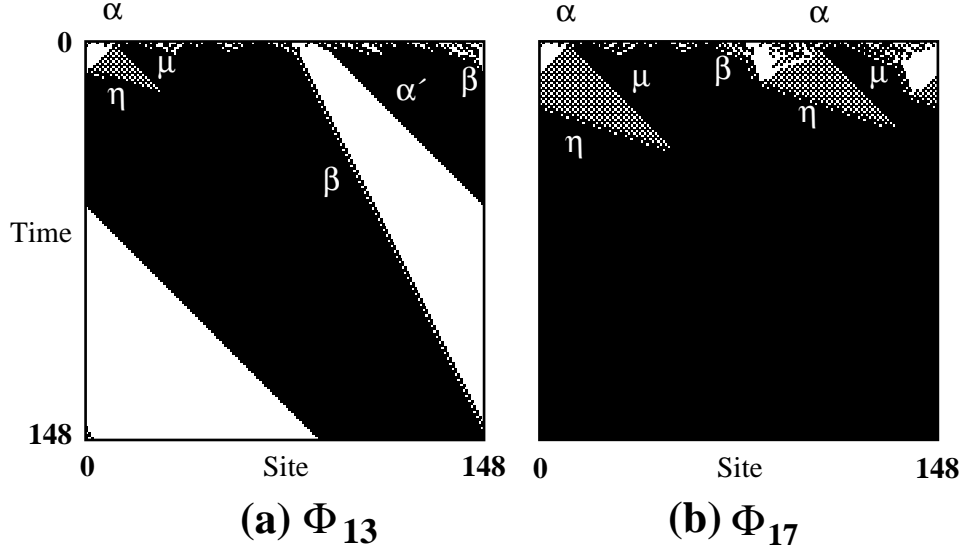


Figure 16: Space-time behavior of $\phi_{\text{par}}^{\text{a}}$ ancestors, ϕ_{13} and ϕ_{17} arising in generation 13 and 17. Both start from the same IC with $\rho_0 = 0.58$.

Fig. 15(b). We determined, in a fashion similar to that just explained above, that these traits also were adaptively neutral.

8.3 ϕ_{13} and ϕ_{17} (Fig. 16)

Here $\rho_0 = 0.58$. ϕ_{13} expands blocks of 0s on many ICs with $\rho > 1/2$, including the one in this figure, resulting in misclassifications. In fact, many high-density ICs with $\rho \approx 0.5$ are misclassified and, while ϕ_{13} has markedly higher F_{149}^{100} than its ancestors, its performance $\mathcal{P}_{149}^{10^4}$ is only marginally improved (see Table 5).

ϕ_{13} creates three types of boundaries between white and black domains. Two of them are shown in Fig. 16(a), labeled α and α' . The α , like $\phi_{\text{par}}^{\text{a}}$'s α , exists for only a single time step and then decays into η and μ , whereas α' remains stable. A third type, α'' , does not appear for this IC but can be seen in Fig. 15(b). α' and α'' support the block-expanding strategy, whereas α leads to a competition between white and black regions similar to that seen in $\phi_{\text{par}}^{\text{a}}$.

In contrast, consider Fig. 16(b), where the same $\rho = 0.58$ IC is correctly classified by ϕ_{17} . Recalling Table 5 we see that ϕ_{17} 's F_{149}^{100} and $\mathcal{P}_{149}^{10^4}$ are both substantially higher than those of ϕ_{13} . ϕ_{17} 's higher F_{149}^{100} and $\mathcal{P}_{149}^{10^4}$ can be explained at the particle level. The particles are labeled in Fig. 16(a) and Fig. 16(b).

ϕ_{17} creates the same set of particles as ϕ_{13} (on some ICs it expands 0-blocks, not shown in Fig. 16(b)) but with different frequencies of occurrence: α' and α'' appear less often than in ϕ_{13} and α appears more often. Thus, ϕ_{13} is more likely to expand 0-blocks, and thus make more errors, than ϕ_{17} on ICs for which $\rho_0 > 0.5$. Given 100 randomly generated $\rho > 0.5$ ICs, α' and α'' were created by ϕ_{13} in 86% of the ICs and by ϕ_{17} in 12% of the ICs. Whenever

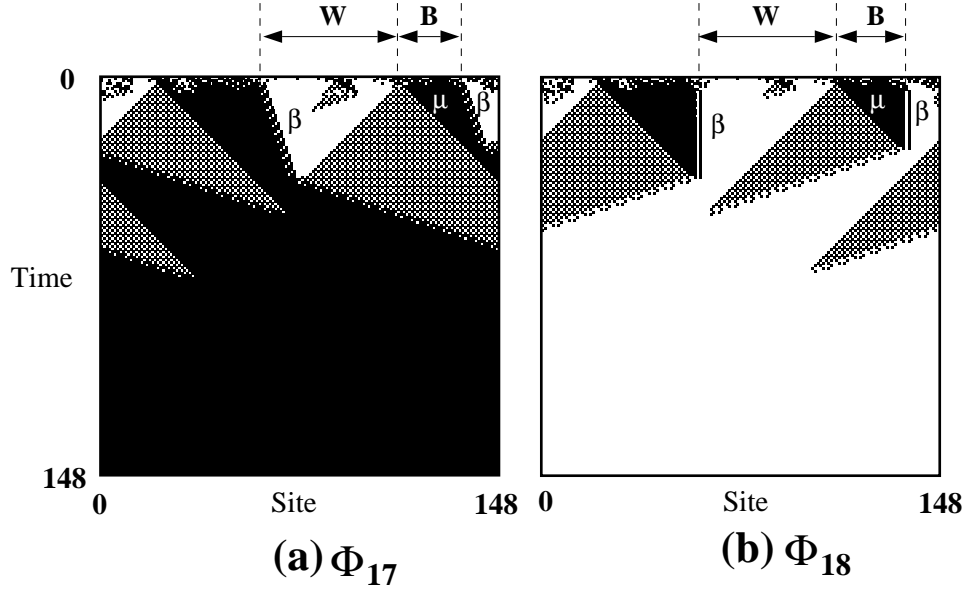


Figure 17: Space-time behavior of generation 17 and 18 ancestors, ϕ_{17} and ϕ_{18} , of ϕ_{par}^a . Both are shown starting from the same IC that has $\rho_0 = 0.45$.

α' or α'' are created, the final configuration will be all 0s regardless of whether α is created. That is, block expanding dominates other behaviors. This explains why flipping output bits to suppress the checkerboard domain does not significantly affect ϕ_{13} 's F_{149}^{100} and $\mathcal{P}_{149}^{10^4}$, but does significantly affect these values for ϕ_{17} . When the checkerboard domain was suppressed in ϕ_{17} , F_{149}^{100} decreased only to 0.86 but $\mathcal{P}_{149}^{10^4}$ decreased to 0.54.

Following Gould and Vrba [36], we consider the checkerboard domain Λ^2 to be an example of an “exaptation”—a trait that has no adaptive significance when it first appears, but is later co-opted by evolution to have adaptive value. According to Gould and Vrba, such traits are common in biological evolution. In the evolutionary innovation that goes from ϕ_{13} to ϕ_{17} the exaptation of Λ^2 in ϕ_{13} makes just this transition to functionality associated with a marked increase in fitness and performance. This, in turn, leads to the change in dominant computational strategy away from block expanding.

8.4 ϕ_{17} and ϕ_{18} (Fig. 17)

Here $\rho_0 = 0.45$. The misclassification by ϕ_{17} (illustrated in Fig. 17(a)) is compared with the correct classification by ϕ_{17} 's higher fitness and performance child ϕ_{18} (Fig. 17(b)). Both CAs create similar particles, but in ϕ_{17} the velocity of the β particle is $1/3$, whereas in ϕ_{18} its velocity is zero.

In Fig. 17(a), the white region (marked **W**) is larger than the black region to its right (marked **B**). Since the β particles have positive velocity, the black regions to **W**'s left and

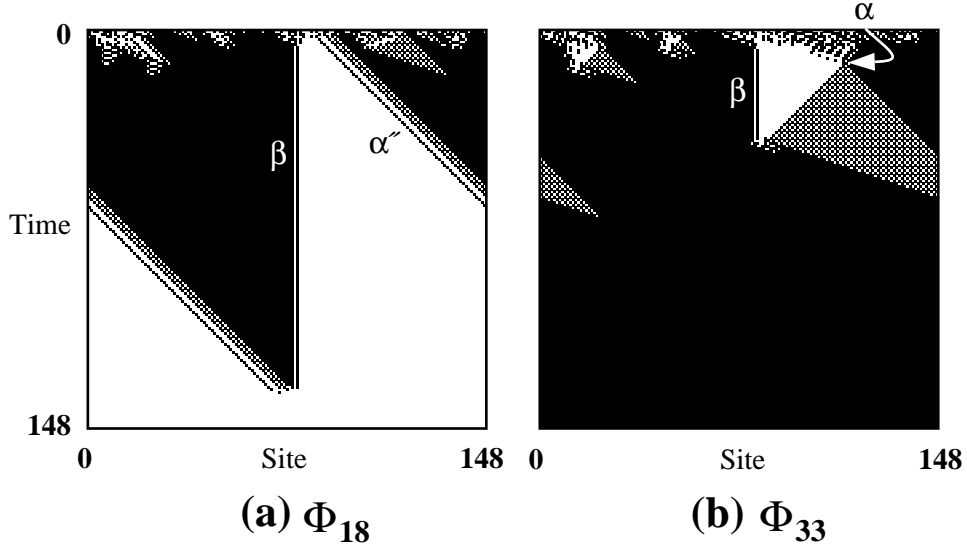


Figure 18: Space-time behavior of generation 18 and 33 ancestors, ϕ_{18} and ϕ_{33} , of $\phi_{\text{par}}^{\text{a}}$. Both start from the same IC with $\rho_0 = 0.61$.

right both expand to the right. Coming in from the left, this decreases the size of \mathbf{W} . On the other side, the (rightmost) β particle moves away from the \mathbf{W} region. This asymmetry allows the \mathbf{B} region to win the size competition, when the \mathbf{B} region should not.

The asymmetry between black and white regions is corrected in ϕ_{18} by the change in β 's velocity to zero. This makes the size competition between black and white regions symmetric. The result, seen in Fig. 17(b), is that the smaller \mathbf{B} region is now cut off by the μ and β , the \mathbf{W} region is allowed to grow, and the correct classification is made.

8.5 ϕ_{18} and ϕ_{33} (Fig. 18)

Here $\rho_0 = 0.61$. ϕ_{18} , though an improvement over ϕ_{17} , still carries with it remnants of its ancestors' block-expanding past. In Fig. 18(a), ϕ_{18} misclassifies the IC by creating an α'' particle instead of an α particle at a white-black (ambiguous density) boundary in the IC. Recall that in ϕ_{17} , α' or α'' particles were created in 12% of the random ICs with $\rho > 1/2$. In ϕ_{18} this frequency is about the same: 13%. Thus, ϕ_{18} 's main innovation over ϕ_{17} is the zero velocity of the β particle and the resulting symmetric size-competition strategy.

In ϕ_{33} , a descendant of ϕ_{18} , neither α' or α'' particles are created. This explains the higher F_{149}^{100} and $\mathcal{P}_{149}^{10^4}$ of ϕ_{33} over those of ϕ_{18} .

8.6 ϕ_{33} and ϕ_{64} (Fig. 19)

Here, $\rho_0 = 0.45$. $\phi_{\text{par}}^{\text{a}}$, here named ϕ_{64} to denote its generation of birth, outperforms ϕ_{33} since it classifies more low-density ICs correctly. On some low-density ICs like the one used in Fig. 19(a), ϕ_{33} condenses too much of the IC into black regions, a type 1 error. These

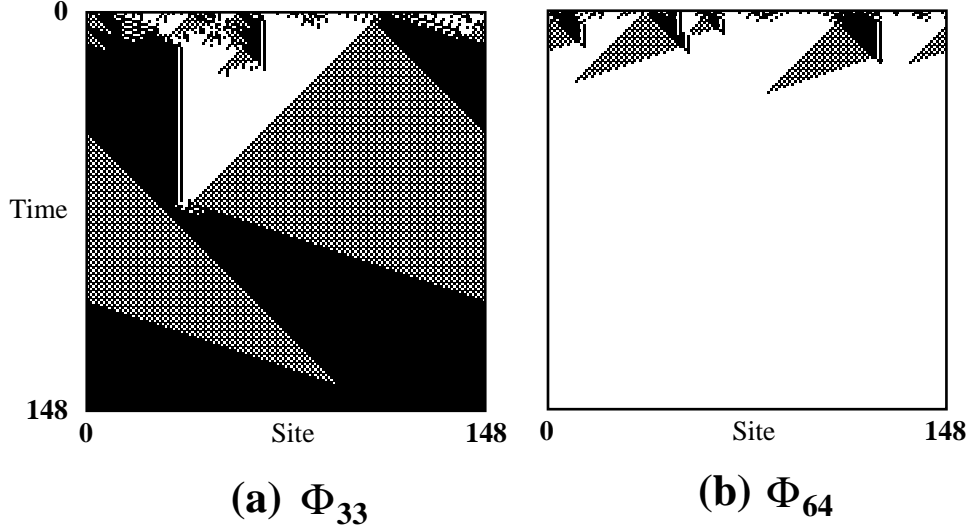


Figure 19: Space-time behavior of generation 33 ancestor ϕ_{33} of $\phi_{\text{par}}^{\text{a}}$ and ϕ_{64} (itself $\phi_{\text{par}}^{\text{a}}$). Both start from the same IC, which has density $\rho_0 = 0.45$.

then win the size competition, resulting in a misclassification. ϕ_{64} makes type 1 errors on low-density ICs less often (e.g., as seen in Fig. 19(b)), it correctly classifies the same IC as in Fig. 19(a). On the same set of 10^4 ICs, 62% of ϕ_{33} 's errors were on low-density ICs, whereas only 43% of ϕ_{64} 's errors were on low-density ICs.

8.7 Particle Models of Evolved Cellular Automata

The “natural history” of $\phi_{\text{par}}^{\text{a}}$'s evolution given above demonstrates how we can understand the jumps in F_{149}^{100} and $\mathcal{P}_{149}^{10^4}$ in terms of regular domains and particles—functional components in the CA's dynamical behavior. The GA's actions can be described at a low level as manipulating bits in CA rule tables via crossover and mutation, but a better understanding of the evolutionary process emerges when we describe its actions at the higher level of manipulating particle types, velocities, and interactions. An important component of this viewpoint is that the particles and their interactions lead to higher fitness. To test the hypothesis more quantitatively, we ask to what extent the CAs' observed fitnesses and performances can be predicted from the particle and interaction properties alone. To this end, in collaboration with Wim Hordijk, we have constructed “ballistic” particle models of the CAs ϕ_8 through ϕ_{64} . These models are intended to isolate the particle-level mechanisms and in so doing allow us to determine how much of the CA behavior this level captures.

A ballistic particle model \mathcal{M}_ϕ of a CA ϕ consists of the catalog of particle types, velocities, interactions, and their frequencies of occurrence at t_c . \mathcal{M}_ϕ is “run” by first using the particle frequencies to generate an initial configuration \mathbf{s}_{t_c} of particles at the condensation time and then using the catalog of velocities and interactions to calculate the initial particles' ballistic trajectories and the products of subsequent particle interactions. The final

configuration is reached when either all particles have annihilated or when $T_{\max} - t_c$ steps have occurred. This configuration and the actual time at which it was reached gives us \mathcal{M}_ϕ 's prediction of what ϕ 's classification would be for an IC corresponding to \mathbf{s}_{t_c} and the time it would take ϕ to reach it. Particle models and their analysis are described in detail in Refs. [16] and [42].

CA Name	$\mathcal{P}_{149}^{10^4}(\phi)$	$\mathcal{P}_{149}^{10^4}(\mathcal{M}_\phi)$
ϕ_8	0.500	0.500
ϕ_{13}	0.513	0.524
ϕ_{17}	0.595	0.601
ϕ_{18}	0.691	0.747
ϕ_{33}	0.735	0.765
ϕ_{64}	0.775	0.775

Table 6: The CA and model performances $\mathcal{P}_{10^4}^{149}$ of ϕ_8 , ϕ_{13} , ϕ_{17} , ϕ_{18} , ϕ_{33} , and ϕ_{64} . (After [16].) Note ϕ_{par}^a has been referred here as ϕ_{64} . The CA rule tables are given in Table 5.

A comparison of the performances of the six CAs just analyzed and their particle models are given in Table 6. As can be seen, the agreement is within a few percent for most cases. In these and the other cases small discrepancies are due to simplifications made in the particle models. These include assumptions such as the particles being zero width and interactions occurring instantaneously. These error sources are analyzed in depth in Ref. [16]. For ϕ_{18} the error is higher, around 8%, due to a long-lived transient domain that is not part of the particle catalog used for the model. The main effect of this is that the condensation time is overestimated on some ICs that generate this domain. This, in turn, means that the model describes only the last stages of convergence to the answer configurations, which it gets correctly and so has a higher performance than ϕ_{18} . For ϕ_{33} the error is around 4%. This appears to be due to errors in estimates of the distribution of particle types at the condensation time.

The conclusion is that the particle-level descriptions can be used to quantitatively predict the computational behavior of CAs and so also the CA fitnesses and performances in the evolutionary setting. In particular, the results support the claim that it is these higher-level structures, embedded in CA configurations, that implement the CA's computational strategy. More germane to the preceding natural history analysis, this level of description allows us to understand at a functional level of structural components the evolutionary process by which the CAs were produced.

9. Related Work

In Sec. 3 we discussed some similarities and differences between this work and other work on distributed parallel computation. In this section we examine relationships between this work and other work on computation in cellular automata.

It should be pointed out that ϕ_{par}^a 's behavior (and the behavior of many of the other highest-performance rules) is very similar to the behavior of the so-called Gács-Kurdyumov-Levin (GKL) CA. This CA was invented not to perform the $\rho_c = 1/2$ task, but to study reliable computation and phase transitions in one-dimensional spatially-extended systems [33]. More extensive work by Gács on reliable computation with CAs is reported in Ref. [34].

The present work and earlier work by our group came out of follow-on research to Packard's investigation of "computation at the edge of chaos" in cellular automata [60]. Originally Wolfram proposed a classification of CAs into four behavioral categories [81]. These categories followed the basic classification of dissipative dynamical systems: fixed point attractors exhibiting equilibrium behavior, limit cycle attractors exhibiting periodic behavior, chaotic attractors exhibiting apparently random behavior, and neutrally stable systems at bifurcations exhibiting long transients. Wolfram suggested that the latter category was particularly appropriate for implementing sophisticated (even universal) computation.

Following this with a more quantitative proposal Langton [49] hypothesized that a CA's λ —the fraction of "non-quiescent states" (here, 1s) in its look-up table's output states—was correlated "generically" with the CA's computational capabilities. In particular, he hypothesized that CAs with certain "critical" λ values, which we denoted λ_c , would be more likely than CAs with λ values away from λ_c to be able to perform complex computations, or even universal computation. Packard's goal was to test this hypothesis by using a genetic algorithm to evolve $(k, r) = (2, 3)$ CAs to perform the $\rho_c = 1/2$ task, starting from an initial population chosen from a distribution that was uniform over $\lambda \in [0, 1]$. He found that after 100 generations, the final populations of CAs, when viewed only as distributions over λ , tended to cluster close to λ_c values. He interpreted this clustering as evidence for the hypothesized connection between λ_c and computational ability.

In Ref. [57] we were able to show, via theoretical arguments and empirical results, however, that the most successful CAs for the $\rho_c = 1/2$ task must have $\lambda \approx 1/2$. This value of λ is quite different from Packard's quoted λ_c values. We argued that Packard's results were due to an artifact in his particular implementation of the GA. Using more standard versions and his version of GA search we obtained results that disagreed with Packard's findings and that were roughly in accord with our theoretical predictions that high performance CAs were to be found at $\lambda \approx 1/2$, far from λ_c , and not in, for example, Wolfram's fourth CA category. We were also able to explain the deviations of our results from the theoretical predictions. The current work came out of the discovery of phenomena, such as embedded-particle CAs [17, 20], that were not found in Ref. [60]. Moreover, according to Langton the $\lambda = 1/2$ value for our high-performance CAs corresponds to CAs in Wolfram's chaotic class. The space-time diagrams shown earlier demonstrate that they are not "chaotic"; their behavior, in fact, puts them in the first (fixed-point) category.

Later, other researchers performed their own studies of evolving cellular automata for the $\rho_c = 1/2$ task. Sipper and Ruppin [65, 66] used a version of the GA to evolve "nonuniform CAs"—CA-like architectures in which each cell uses its own look-up table to determine its state at each time step. For a lattice of size N , the individuals in the GA population are the N look-up tables making up a nonuniform CA. Sipper and Ruppin used this framework to evolve $r = 1$ nonuniform CAs to perform the $\rho_c = 1/2$ task, as well as other tasks. They

reported the discovery of nonuniform CAs with $\mathcal{P}_{149}^{10^4}$ values comparable to that of $\phi_{\text{par}}^{\text{a}}$. They did not report $\mathcal{P}_N^{10^4}$ results for any other value of N nor did they give statistics on how often high-performance nonuniform CAs were evolved. Moreover, no structural analysis of CA space-time behavior or GA population dynamics was given. Thus, it is unclear how the high fitnesses were obtained, either dynamically or evolutionarily.

Andre et al. used a genetic programming algorithm to evolve $(k, r) = (2, 3)$ CAs with $N = 149$ to perform the $\rho_c = 1/2$ task [1]. This algorithm discovered particle CAs with higher $\mathcal{P}_{149}^{10^4}$ than that of $\phi_{\text{par}}^{\text{a}}$ (e.g., 0.828 versus 0.776). We obtained the look-up table for one such CA, ϕ_{GP} (D. Andre, personal communication) and found that on larger lattices, the performance of ϕ_{GP} was close to that of $\phi_{\text{par}}^{\text{a}}$ ($\mathcal{P}_{599}^{10^4}(\phi_{\text{GP}}) = 0.765$ and $\mathcal{P}_{999}^{10^4}(\phi_{\text{GP}}) = 0.723$; cf. Table 1). It is not clear whether the improvement in $\mathcal{P}_{149}^{10^4}$ was due to the genetic programming representation CA look-up tables or some other factor related to increased computational resources. For example, their runs had a 500-fold larger population size M and 10-fold larger number of ICs over our GA runs. Their runs did, however, find high-performance CA in average numbers of generations that were half those in our GA. Thus, the computational resources they used in their evolutionary search were approximately 2500 times larger than in our GA runs.

Paredis [62] and Juillé and Pollack [45] experimented with coevolutionary learning techniques to improve the GA's search efficiency to find embedded particle CAs for the $\rho_c = 1/2$ task. The latter work specifically rewarded or penalized ICs of particular densities, depending on the amount of information ICs of those densities provided for distinguishing fitnesses between CAs in the population. This resulted in a higher percentage of GA runs in which high-performance embedded-particle CAs were discovered and in the discovery of higher-performance CAs than in any of the non-coevolutionary runs. The highest performance CA discovered had $\mathcal{P}_{10^5}^{149} = 0.863 \pm 0.001$, $\mathcal{P}_{10^5}^{599} = 0.822 \pm 0.001$, and $\mathcal{P}_{10^5}^{999} = 0.804 \pm 0.001$. Unfortunately, the performance of this coevolved CA, although high on small lattices (e.g. $N = 149$), decays more rapidly with lattice size than the GKL rule, which happens to have lower performance than the coevolved rule on small lattices. This appears to be the result of the more complex domains that preclude, through additional persistent particles, convergence to the answer configurations, 0^N or 1^N . Compared to the coevolved CAs, the GKL CA is one of the CAs that maintains high performance on larger lattices.

Our own work has been extended to other tasks, most thoroughly to a global synchronization task for which we have performed similar analyses to those given in this paper [19].

Our notion of computation via particles and particle-interactions derives from that introduced by the computational mechanics framework [12, 38, 39] and so differs considerably from the notions used in most other work on designing CAs for computation. For example, propagating particle-like signals were used in the solution to the Firing Squad Synchronization Problem [52, 58, 77], in Smith's work on CAs for parallel formal-language recognition [68], and in Mazoyer's work on computation in one-dimensional CAs [53]. However, in all these cases, the particles and their interactions were designed by hand to be the explicit behavior of the CA. That is, the particles are explicitly coded in each cell's local state and their dynamics and their interactions are coded directly into the CA lookup table. Typically, their interactions were effected by a relatively large number of states per site. Steiglitz, Kamal,

and Watson’s carry-ripple adder [70] and the universal computer constructed in the Game of Life [3] both used binary-state signals consisting of propagating periodic patterns. But, again, the particles were explicitly designed to ride on top of a quiescent background and their interaction properties were carefully hand coded. In Squier and Steiglitz’s “particle machine” [69] and in Jakubowski, Steiglitz, and Squier’s “soliton machine” [43], particles are the primitive states of the CA cells. Moreover, their interaction properties are explicitly given by the CA rule table. These machines are essentially kinds of lattice gas automata [23] that operate on “particles” directly. (Other work on arithmetic in cellular automata has been done by Sheth, Nag, and Hellwarth [64] and Clementi, De Biase, and Massini [8], among others.)

In contrast to these, particles in our system are embedded as walls between regular domains. They are often apparent only after those domains have been discovered and filtered out. Their structures and interaction properties are emergent properties of the patterns formed by the CAs. Notably, although each cell has only two possible states, the structures of embedded particles are spatially and temporally extended, and so are more complex than atomic or simple periodic structures. Typically, these structures can extend over spatial scales larger than the CA radius. For example, the background domain of the elementary CA (ECA 110) shown in Fig. 2 has a temporal periodicity of 7 time steps and a spatial periodicity of 14 sites, markedly larger than the $r = 1$ nearest-neighbor coupling.

10. Conclusion

Our philosophy is to view CAs as systems that naturally form patterns (such as regular domains) and to view the GA as taking advantage—via selection and genetic variation—of these pattern-forming propensities so as to shape them to perform desired computations. Within this framework, we attempt to understand the behavior of the resulting CAs by applying tools, such as the computational mechanics framework, formulated for analyzing pattern-forming systems. The result gives us a high-level description of the computationally relevant parts of the system’s behavior. In doing so, we begin to answer Wolfram’s last problem from “Twenty problems in the theory of cellular automata” (Wolfram, 1985): “What higher-level descriptions of information processing in cellular automata can be given?” We believe that this framework will be a basis for the “radically new approach” that Wolfram claimed will be required for understanding and designing sophisticated computation in CAs and other decentralized spatially extended systems.

Our analysis showed that there are three levels of information processing occurring during iterations of the evolved high-performance CAs. The first was the type of information storage and transmission effected by the particles and the type of “logical” operations implemented by the particle interactions. The second, higher level comprised the geometric subroutines that implemented intermediate-scale computations. We analyzed in detail two of these that were important to the size competition between regions of low and high density. We also showed how variations in the particles led to several types of error at this level. The third and final level is that of the global computation over the entire lattice up to the answer time. This is the level at which fitness is conferred on the CAs.

We analyzed in some detail the natural history that led to the emergence of such com-

putationally sophisticated CAs. The evolutionary epochs typically proceed in a set sequence, with earlier epochs setting the (necessary) context for the later, higher performance ones. Often the jumps to higher epochs were facilitated by exaptations—changes in adaptively neutral traits appearing in much earlier generations.

There are a number of fruitful directions for future work. The first is to extend the lessons learned here to more general evolutionary search algorithms and pattern forming dynamical systems. The problem of choosing a genetic representation of dynamical systems that helps, or at least does not hinder, the search will play an important role in addressing this. The evolution of CAs that operate on two-dimensional images rather than one-dimensional strings will also help address this issue and also open up application areas, such as iterative nonlinear image processing [11].

We also need to develop substantially better analytical descriptions of the search’s population dynamics and of how the intrinsic structures in CAs interact with that dynamics. Although the evolution of CAs is a very simplified problem from the biological perspective, the evolutionary time scale of the population dynamics and the development time scale of the CAs result in a two-time-scale stochastic dynamical system that is difficult to analytically predict. Such predictions, say of how to set the mutation rate or population size for effective search, are centrally important both for basic understanding of evolutionary mechanisms and for practical applications. Progress on quantitatively predicting the population dynamics occurring during epochal evolution has been made [73, 74]. The adaptation of the “statistical dynamics” approach introduced there to the evolution of CAs will be an important, but difficult, step toward understanding complicated genotype-to-phenotype maps. The latter is highly relevant for using such search methods on complex problems.

Another quantitative direction is the estimation of computational performance of distributed systems based on higher-level descriptions. The results, reported here and described in detail in Refs. [16] and [42], on predicting CA computational performance are encouraging. Constructing a more accurate model along with a quantitative analytical model of higher-level computation in CAs will help us understand how much the embedded CA structures contribute individually to overall fitness. And this, in turn, will allow us to monitor the evolutionary mechanisms that lead to the emergence of collective computation in coordinated groups of functional units.

Acknowledgments

The authors thank Wim Hordijk for calculating the CA particle-model performances and Silas Alben for calculating the coevolved CA performances. They also thank Jim Hanson, Wim Hordijk, Cris Moore, Erik van Nimwegen, and Cosma Shalizi for helpful discussions. This work was supported at UC Berkeley by ONR grant N00014-95-1-0524 and at the Santa Fe Institute by ONR grant N00014-95-1-0975, Sandia National Laboratory contract AU-4978, and National Science Foundation grant IRI-9705853.

A. Domain Filter

In this appendix we describe the properties and construction of $\phi_{\text{par}}^{\text{a}}$'s domain-recognizing and filtering transducer.

The transducer, shown in Fig. 20, reads in binary CA configurations and outputs strings of the same length, the lattice size N , in the domain-wall alphabet $\{\lambda, 0, 1, 2, w\}$. In this alphabet λ indicates that the transducer has not yet “synchronized” (see below) to the domain or wall structures in the configuration, $\{0, 1, 2\}$ label each of the three domains, respectively, and w indicates a wall between domains. In the filtered space-time diagrams w is mapped to black and all other output symbols map to white.

Briefly, $\phi_{\text{par}}^{\text{a}}$'s domain-wall transducer is constructed as follows. $\phi_{\text{par}}^{\text{a}}$ has three domains, each of which can be described by simple finite-state machines. These machines form the recurrent states of the transducer. When the transducer first begins to read in the configuration, it may take several steps to disambiguate the site values and identify the appropriate domain in which they are participating. Working through the transitions and transient states that lead to the recurrent (domain) states determines the transitions from the start state. When the transducer is reading site values consistent with one of these domains, but then encounters site values that are not consistent with it (e.g. values indicating walls), then some number of additional site values must be read in to determine the domain type into which the transducer has moved. Such transitions determine the transducer's domain-to-domain transitions.

Note, that due to the steps required to initially read in a sufficient number of site values to recognize the domains and walls, a process that we call synchronization, the transducer may have to read some portion of the configuration that it has already read, as it wraps around due to the lattice's periodic boundary conditions. This takes at most one additional pass over the configuration.

The general construction procedure for domain-wall transducers is given in Ref. [15].

References

- [1] D. Andre, F. H. Bennett III, and J. R. Koza. Evolution of intricate long-distance communication signals in cellular automata using genetic programming. In *Artificial Life V: Proceedings of the Fifth International Workshop on the Synthesis and Simulation of Living Systems*, Cambridge, MA, 1996. MIT Press.
- [2] T. Bäck. *Evolutionary Algorithms in Theory and Practice: Evolution Strategies, Evolutionary Programming, Genetic Algorithms*. Oxford University Press, Oxford, 1996.
- [3] E. Berlekamp, J. H. Conway, and R. Guy. *Winning Ways For Your Mathematical Plays*, volume 2. Academic Press, New York, NY, 1982.
- [4] A. W. Burks, editor. *Essays on Cellular Automata*. University of Illinois Press, Urbana, IL, 1970.
- [5] M. S. Capcarrere, M. Sipper, and M. Tomassini. Two-state, $r=1$ cellular automaton that classifies density. *Physical Review Letters*, 77(24):4969–4971, 1996.

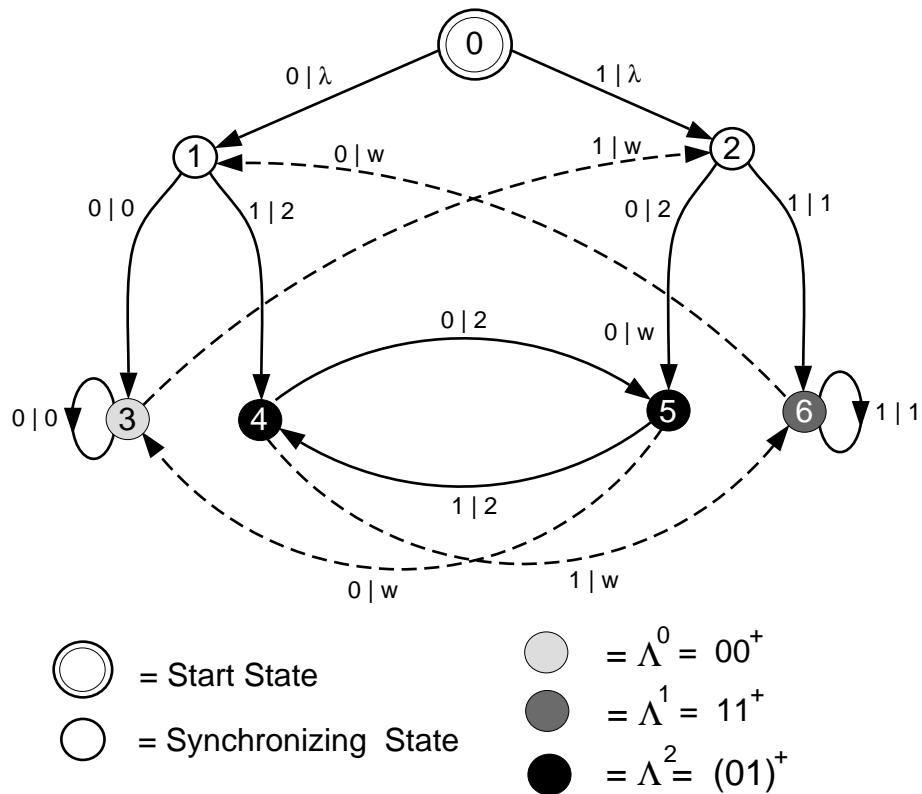


Figure 20: ϕ_{par}^a 's domain-recognizing and filtering transducer. The edge labels $s|t$ indicate that the transition is to be taken on reading configuration site value $s \in \{0, 1\}$ and then outputting structural label $t \in \{\lambda, 0, 1, 2, w\}$.

- [6] H. F. Chau, K. K. Yan, K. Y. Wan, and L. W. Siu. Classifying rational densities using two one-dimensional cellular automata. *Physical Review E*, 57(2A):1367–1369, 1998.
- [7] P. S. Churchland and T. J. Sejnowski, editors. *The Computational Brain*. MIT Press, Cambridge, MA, 1992.
- [8] A. Clementi, G. A. De Biase, and A. Massini. Fast parallel arithmetic on cellular automata. *Complex Systems*, 8(6):435, 1994.
- [9] A. Colorni, M. Dorigo, and V. Maniezzo. Distributed optimization by ant colonies. In F. J. Varela and P. Bourguine, editors, *Toward a Practice of Autonomous Systems: Proceedings of the First European Conference on Artificial Life*, pages 134–142, Cambridge, MA, 1992. MIT Press/Bradford Books.
- [10] J. M. Crichlow. *An Introduction to Distributed and Parallel Computing*. Prentice Hall, London, 1997.
- [11] J. P. Crutchfield. Spatio-temporal complexity in nonlinear image processing. *IEEE Trans. Circ. Sys.*, 37:770, 1988.
- [12] J. P. Crutchfield. The calculi of emergence: Computation, dynamics, and induction. *Physica D*, 75:11–54, 1994.
- [13] J. P. Crutchfield. Is anything ever new? Considering emergence. In G. Cowan, D. Pines, and D. Melzner, editors, *Complexity: Metaphors, Models, and Reality*, volume XIX of *Santa Fe Institute Studies in the Sciences of Complexity*, Reading, MA, 1994. Addison-Wesley. In press.
- [14] J. P. Crutchfield and J. E. Hanson. Attractor vicinity decay for a cellular automaton. *CHAOS*, 3(2):215–224, 1993.
- [15] J. P. Crutchfield and J. E. Hanson. Turbulent pattern bases for cellular automata. *Physica D*, 69:279–301, 1993.
- [16] J. P. Crutchfield, W. Hordijk, and M. Mitchell. Predicting the behavior of evolved cellular automata. Manuscript in preparation.
- [17] J. P. Crutchfield and M. Mitchell. The evolution of emergent computation. *Proceedings of the National Academy of Science U.S.A.*, 92:10742–10746, 1995.
- [18] R. Das. *The Evolution of Emergent Computation in Cellular Automata*. PhD thesis, The Colorado State University, Fort Collins, CO, 1998.
- [19] R. Das, J. P. Crutchfield, M. Mitchell, and J. E. Hanson. Evolving globally synchronized cellular automata. In L. J. Eshelman, editor, *Proceedings of the Sixth International Conference on Genetic Algorithms*, pages 336–343, San Francisco, CA, 1995. Morgan Kaufmann.
- [20] R. Das, M. Mitchell, and J. P. Crutchfield. A genetic algorithm discovers particle-based computation in cellular automata. In Y. Davidor, H.-P. Schwefel, and R. Männer, editors, *Parallel Problem Solving from Nature—PPSN III*, volume 866, pages 344–353, Berlin, 1994. Springer-Verlag (Lecture Notes in Computer Science).

- [21] J. L. Deneubourg, S. Goss, N Franks, A. Sendova-Franks, C. Detrain, and L. Chrétien. The dynamics of collective sorting: Robot-like ants and ant-like robots. In J.-A. Meyer and S. W. Wilson, editors, *From Animals To Animats: Proceedings of the First International Conference on Simulation of Adaptive Behavior*, pages 356–363, Cambridge, MA, 1991. MIT Press.
- [22] D. Dolev and H. R. Strong. Authenticated algorithms for Byzantine agreement. *SIAM Journal of Computing*, 12(4):656–666, 1983.
- [23] G. Doolen. *Lattice Gas Methods for Partial Differential Equations*. Addison-Wesley, Reading, MA, 1990.
- [24] K. Eloranta. The dynamics of defect ensembles in one-dimensional cellular automata. *Journal of Statistical Physics*, 76(5/6):1377, 1994.
- [25] D. Farmer, T. Toffoli, and S. Wolfram, editors. *Cellular Automata: Proceedings of an Interdisciplinary Workshop*. North Holland, Amsterdam, 1984.
- [26] J. D. Farmer, N. H. Packard, and A. S. Perelson. The immune system, adaptation, and machine learning. *Physica D*, 22:187–204, 1986.
- [27] A. A. Farrag and R. J. Dawson. On designing efficient consensus protocols. In M. H. Barton, E. L. Dagless, and G. L. Reijns, editors, *Distributed Processing*, pages 413–427, Amsterdam, 1988. Elsevier Science Publishers.
- [28] E. Fiesler and R. Beale, editors. *Handbook of Neural Computation*. Oxford University Press, New York, 1997.
- [29] D. B. Fogel. *Evolutionary Computation: Toward a New Philosophy of Machine Intelligence*. IEEE Press, New York, 1995.
- [30] F. Fogelman-Soulie, Y. Robert, and M. Tchuente, editors. *Automata Networks in Computer Science: Theory and Applications*. Manchester University Press, Manchester, UK, 1987.
- [31] S. Forrest, S. Hofmeyr, and A. Somayaji. Computer immunology. *Communications of the ACM*, 1997. In press.
- [32] H. Fukú. Solution of the density classification problem with two cellular automata rules. *Physical Review E*, 55(3):R2081–R2084, 1997.
- [33] P. Gács. Nonergodic one-dimensional media and reliable computation. *Contemporary Mathematics*, 41:125, 1985.
- [34] P. Gács. Reliable computation with cellular automata. *Journal of Computer and System Sciences*, 32:15–78, 1986.
- [35] D. E. Goldberg. *Genetic Algorithms in Search, Optimization, and Machine Learning*. Addison-Wesley, Reading, MA, 1989.
- [36] S. J. Gould and E. S. Vrba. Exaptation: A missing term in the science of form. *Paleobiology*, 8:4–15, 1982.
- [37] H. A. Gutowitz, editor. *Cellular Automata*. MIT Press, Cambridge, MA, 1990.

- [38] J. E. Hanson. *Computational Mechanics of Cellular Automata*. PhD thesis, University of California at Berkeley, Berkeley, CA, 1993.
- [39] J. E. Hanson and J. P. Crutchfield. The attractor-basin portrait of a cellular automaton. *J. Stat. Phys.*, 66:1415, 1992.
- [40] J. H. Holland. *Adaptation in Natural and Artificial Systems*. MIT Press, Cambridge, MA, 1992. Second edition (First edition, 1975).
- [41] J. E. Hopcroft and J. D. Ullman. *Introduction to Automata Theory, Languages, and Computation*. Addison-Wesley, Reading, 1979.
- [42] W. Hordijk, J. P. Crutchfield, and M. Mitchell. Mechanisms of emergent computation in cellular automata. In *Parallel Problem Solving from Nature—Proceedings Vth Workshop PPSN V*, 1998. To appear.
- [43] M. H. Jakubowski, K. Steiglitz, and R. K. Squier. When can solitons compute? *Complex Systems*, 1996. In press.
- [44] C. Jesshope, V. Jossifov, and W. Wilhelmi, editors. *International Workshop on Parallel Processing by Cellular Automata and Arrays (Parcella '94)*. Akademie Verlag, Berlin, 1994.
- [45] H. Juillé and J. B. Pollack. Coevolutionary learning: A case study. In *Proceedings of the Fifteenth International Conference on Machine Learning*, 1998.
- [46] T. Karapiperis and B. Blankleider. Cellular automaton model of reaction-transport processes. *Physica D*, 78:30–64, 1994.
- [47] H. T. Kung. Why systolic architectures? *Computer*, 15(1):37–46, 1982.
- [48] M. Land and R. K. Belew. No perfect two-state cellular automata for density classification exists. *Physical Review Letters*, 74(25):5148, 1995.
- [49] C. G. Langton. Computation at the edge of chaos: Phase transitions and emergent computation. *Physica D*, 42:12–37, 1990.
- [50] K. Lindgren and M. G. Nordahl. Universal computation in a simple one-dimensional cellular automaton. *Complex Systems*, 4:299–318, 1990.
- [51] D. Marr, editor. *Vision: A Computational Investigation Into the Human Representation and Processing of Visual Information*. W.H. Freeman, San Francisco, 1982.
- [52] J. Mazoyer. An overview of the firing squad synchronization problem. In C. Choffurt, editor, *Automata Networks*. Springer-Verlag, 1988.
- [53] J. Mazoyer. Computations on one-dimensional cellular automata. *Annals of Mathematics and Artificial Intelligence*, 16:1–4, 1996.
- [54] M. Mitchell. *An Introduction to Genetic Algorithms*. MIT Press, Cambridge, MA, 1996.
- [55] M. Mitchell. Computation in cellular automata: A selected review. In T. Gramss, editor, *Nonstandard Computation*, Weinheim, 1998. VCH Verlagsgesellschaft.
- [56] M. Mitchell, J. P. Crutchfield, and P. T. Hraber. Evolving cellular automata to perform computations: Mechanisms and impediments. *Physica D*, 75:361 – 391, 1994.

- [57] M. Mitchell, P. T. Hraber, and J. P. Crutchfield. Revisiting the edge of chaos: Evolving cellular automata to perform computations. *Complex Systems*, 7:89–130, 1993.
- [58] E. F. Moore. The firing squad synchronization problem. In E. F. Moore, editor, *Sequential Machines: Selected Papers*, Reading, MA, 1964. Addison-Wesley.
- [59] K. Nagel. Particle hopping models and traffic flow theory. *Phys. Rev. E*, 53:4655–4672, 1996.
- [60] N. H. Packard. Adaptation toward the edge of chaos. In J. A. S. Kelso, A. J. Mandell, and M. F. Shlesinger, editors, *Dynamic Patterns in Complex Systems*, pages 293–301, Singapore, 1988. World Scientific.
- [61] N. H. Packard. Intrinsic adaptation in a simple model for evolution. In C. G. Langton, editor, *Artificial Life*, pages 141–155, Reading, MA, 1989. Addison-Wesley.
- [62] J. Paredis. Coevolving cellular automata: Be aware of the red quen! In T. Bäck, editor, *Proceedings of the Seventh International Conference on Genetic Algorithms*, pages 393–400, San Francisco: CA, 1997. Morgan Kaufmann.
- [63] D. E. Rumelhart, G. E. Hinton, and J. L. McClelland. A general framework for parallel distributed processing. In D. E. Rumelhart, J. L. McClelland, and the PDP Research Group, editors, *Parallel Distributed Processing*, volume 1, pages 45–76, Cambridge, MA, 1986. MIT Press.
- [64] B. Sheth, P. Nag, and R. W. Hellwarth. Binary addition on cellular automata. *Complex Systems*, 5:479, 1991.
- [65] M. Sipper. *Evolution of Parallel Cellular Machines: The Cellular Programming Approach*. Springer, Berlin, 1997.
- [66] M. Sipper and Eytan Ruppín. Co-evolving architectures for cellular machines. *Physica D*, 99:428–441, 1997.
- [67] A. R. Smith. Simple computation-universal cellular spaces. *Journal of the ACM*, 18:339, 1971.
- [68] A. R. Smith. Real-time language recognition by one-dimensional cellular automata. *J. Comput. System Sci.*, 6:233, 1972.
- [69] R. K. Squier and K. Steiglitz. Programmable parallel arithmetic in cellular automata using a particle model. *Complex Systems*, 8:311–323, 1994.
- [70] K. Steiglitz, I. Kamal, and A. Watson. Embedding computation in one-dimensional automata by phase-coding solutions. *IEEE Transactions on Computers*, 37:138–145, 1988.
- [71] T. Toffoli and N. Margolus. *Cellular Automata Machines: A New Environment for Modeling*. MIT Press, Cambridge, MA, 1987.
- [72] A. M. Turing. Computing machinery and intelligence. *Mind*, 59(236), 1950.
- [73] E. van Nimwegen and J. P. Crutchfield. Optimizing epochal evolutionary search: Population-size independent theory. *Computer Methods in Applied Mechanics and Engineering, special issue on Evolutionary and Genetic Algorithms in Computational Mechanics and Engineering*, D. Goldberg, editor, 1998. Submitted. Santa Fe Institute Working Paper 98-06-046, 1998.

- [74] E. van Nimwegen, J. P. Crutchfield, and M. Mitchell. Statistical dynamics of the royal road genetic algorithm. *Theoret. Comp. Sci.*, 1998. To appear. Santa Fe Institute Working Paper 97-04-035, 1997.
- [75] J. von Neumann. *The Computer and the Brain*. Yale University Press, New Haven, CT, 1958.
- [76] J. von Neumann. *Theory of Self-Reproducing Automata*. University of Illinois Press, Urbana, IL, 1966. Edited and completed by A. W. Burks.
- [77] A. Waksman. An optimum solution to the firing squad synchronization problem. *Information and Control*, 9:66–78, 1966.
- [78] C. A. Waldspurger, T. Hogg, B. A. Huberman, J. O. Kephart, and W. S. Stornetta. Spawn: A distributed computational economy. *IEEE Transactions on Software Engineering*, 18(2):103–117, 1992.
- [79] N. Wiener. *Cybernetics, or, Control and Communication in the Animal and the Machine*. John Wiley and Sons, New York, 1948.
- [80] M. P. Wellman. A market-oriented programming environment and its application to distributed multicommodity flow problems. *Journal of Artificial Intelligence Research*, 1:1–23, 1993.
- [81] S. Wolfram. Statistical mechanics of cellular automata. *Review of Modern Physics*, 55:601–644, 1983.
- [82] S. Wolfram, editor. *Theory and Applications of Cellular Automata*. World Scientific, Singapore, 1986.